On the Determination of Elastic and Anelastic Properties of Isotropic Spheres

Martin L. Smith

Originally published:
March 1972
Research Report 299
Cold Regions Research And Engineering Laboratory

Samizdat
Press

Published by the Samizdat Press

Center for Wave Phenomena

Department of Geophysics

Colorado School of Mines

Golden, Colorado 80401

and

New England Research

76 Olcott Drive

White River Junction, Vermont 05001

Release 1.1, February 1997

Abstract

We have presented a self-contained account of the theoretical framework necessary to infer the elastic properties of layered spheres from their forced or free resonance spectra. In support of these results, we have provided numerical and experimental results, limited for external reasons to singly layered bodies. We have also provided graphical aids which enable a rapid and fairly accurated determination of compressional and shear velocities for a homogeneous sphere from a single, particular pair of modes. This technique is useful down to Q's at least as low as 100, although unambiguous interpretation of observed spectra requires recourse to the theoretical spectral amplitudes and application of the interference rules. Theoretical spectral calculations suggest that simple peak-width measurements will not provide the information necessary to infer both compressional and shear attenuations, at least for low-Q materials.

Preface

This report was prepared by 1LT Martin L. Smith, Jr., Geologist, Physical Sciences Branch, Research Division, U.S. Army Cold Regions Research and Engineering Laboratory. The work described is part of an investigation of the propagation of elastic waves in soil materials near the freezing point of water sponsored by the Advanced Research Projects Agency (ARPA Order 1525). This report deals with efforts to measure compressional and shear velocities, and their respective attenuations, from the modes of free vibration of an elastic sphere. An attempt has been made to provide a reasonably complete and self-contained account of the appropriate theory (much of which is tutorial), a useful description of the experimental and data-reduction processes, and some graphical aids to allow manual data reduction. Computer codes are not listed but may be obtained (in Fortran II) from the author.[1]

The author wishes to acknowledge the invaluable guidance and encouragement of Dr. Yoshisuke Nakano, USA CRREL, during these endeavors. Captain Randolph J. Martin III and, more recently, Mr. Robert Arnold, both of USA CRREL, were of great help. Mr. Joseph Przybyla helped with the extensive machine calculations; his consistent efforts saved much time. Professor Francis Birch of Harvard University very graciously discussed his own unpublished research in this area. Dr. David B. Fraser of the Bell Telephone Laboratories, Inc., Murray Hill, N.J., kindly shared his experiences and provided helpful reprints and manuscripts. Professor C. H. Scholz of Columbia University also provided many reprints and manuscripts.

[1] 1996: Code is lost in the mists of time.

Contents

List of Figures

List of Tables

1 Introduction

An elastic sphere whose properties vary, at most, as a function of radius alone is the only bounded three-dimensional body whose *entire* spectrum of free vibrations can be determined exactly. (A quantity is, here, considered to be "determined exactly" if it can be computed as the root of an expression which is composed of a finite number of conventional transcendental functions or which can be evaluated by a one-dimensional numerical integration.) Roughly speaking, this is a consequence of the fact that in any of the three elementary coordinate systems (Cartesian, cylindrical and spherical coordinates) a sphere of the above composition is the only *finite* body which is totally symmetric under two of the three coordinates.

Because the solutions so obtained are not restricted to extremely high or low frequencies or to limiting geometries, as in the case of cylinders and plates, we may reasonably hope to evolve an interferometric technique for inferring compressional and shear velocities from observed resonance spectra. This has, in fact, been done.

The earliest such work is that of Francis Birch (personal communication) which antedates World War II, and is unpublished. The earliest published work is that of Fraser and LeCraw (Fraser & LeCraw, 1964). This pioneer work was done on small (19–24 mm radius) spheres of yttrium gallium garnet and yttrium aluminum garnet. Fraser (Fraser, 1968) (Fraser, 1970) made extensive use of the technique to study the properties of vitreous silica. The techniques presented by Fraser and LeCraw (Fraser & LeCraw, 1964) were also applied by Anderson and Soga (Anderson & Soga, 1966) to very small (0.5 mm) spheres of polycrystalline MgO, by Soga and Anderson (Soga & Anderson, 1967) to two tektites, moldanite and indochinite, and by Anderson *et al.* (Anderson *et al.*, 1970) to very small glass spheres (about 0.5 mm) taken from a sample of lunar fines.

The use of spherical interferometry to infer elastic properties requires that we be able to “invert” a known geometry and a set of observed resonant frequencies into, in the case of a homogeneous sphere, a compressional and a shear velocity. Previous workers have used graphical techniques based upon forward eigenfrequency calculations by Cole and Fraser (unpublished). Although such methods do, in fact, yield high accuracy for geometrically precise, high-Q materials such as vitreous silica (Fraser, 1968), we believe that the development of statistical, relatively objective methods was appropriate for the study of much less ideal materials, such as frozen soils. In later sections we describe, and use, a numerical algorithm for inverting arbitrary sets of data and describe a rough method of estimating uncertainties in the result.

A second obstacle we have encountered in the use of low-Q ($Q < 500$) materials is the difficulty of identifying modes, since many resonances are lost in the “skirts” of others. This difficulty is less pronounced, and may often be absent, with high-Q materials. In relief of this, we have developed the appropriate theory of the forced response of an elastic sphere and utilized it to estimate relative modal amplitudes. These results have been extremely useful in interpreting experimental results.

We have also extended both the forward and inverse algorithms to deal with arbitrarily layered spheres (which still, of course, retain spherical symmetry), in order to admit of jacketed samples. Computer storage limitations presently prohibit multilayer inverse calculations and we do not present here numerical or experimental results on such samples.

In pursuit of various of the above, we develop expressions for the kinetic and various potential energy densities associated with modes of free vibration and show how these are useful in

(a) estimating the effect of compositional perturbations on the eigenspectrum and

(b) partitioning a given mode's lumped Q into compressional and shear Q's.

Coquin (Coquin, 1964b), in an application of his earlier technique (Coquin, 1964a), has also solved the latter problem for a homogeneous sphere by using its characteristic equation. His results, while obtained by a different technique, are fundamentally identical with ours, and could be extended numerically to handle the multilayered version of either (a) or (b) above.

Many of the techniques and results we have utilized are drawn from seismological literature concerned with interpretation of the earth's free oscillations. Particularly lucid theoretical discussions are available in Backus and Gilbert (Backus & Gilbert, 1967) and Dahlen (Dahlen, 1968). The methods detailed by Backus (Backus, 1967) are extremely helpful in problems of this sort and we have made extensive use of them. One of the most useful discussions of the behavior of vibrating systems is presented in Rayleigh's *Theory of Sound* (Rayleigh, 1945), first published in 1877.

2 Elastic Displacement Solutions in Spherical Coordinates

We consider a volume of space filled with an isotropic, homogeneous, linearly elastic medium having Lamé constants λ and μ, and density ρ. We assume the medium to be free of gravitation and other body forces, but allow the existence of one or more surfaces across which tractions may be applied.

Let $\mathbf{u}$ be the displacement field specifying the motion of each particle from its unique rest position. We assume $\mathbf{u}$ to be a first order infinitesimal and do not, in the absence of zeroth order fields, have to distinguish between Eulerian and Lagrangian coordinate systems. Let $\mathbb{T}$ be the elastic stress tensor. If we assume that $\mathbf{u} = \vec{0}$ corresponds to the unstressed state of the medium, $\mathbb{T}$ is given by (Fung, 1965):

$$\mathbb{T} = \lambda(\boldsymbol{\nabla} \cdot \mathbf{u})\mathbb{I} + \mu(\boldsymbol{\nabla}\mathbf{u} + \mathbf{u}\boldsymbol{\nabla}), \tag{1}$$

where $\mathbb{I}$ is the identity tensor. $\boldsymbol{\nabla}\mathbf{u}$ is the gradient tensor of $\mathbf{u}$, and $\mathbf{u}\boldsymbol{\nabla}$ is its transpose.

The conservation of linear momentum leads immediately to the equation of motion,

$$\rho\partial_t^2\mathbf{u} = \boldsymbol{\nabla} \cdot \mathbb{T}. \tag{2}$$

Equation 1 and some standard vector calculus identities convert equation 2 to

$$\rho\partial_t^2\mathbf{u} = (\lambda + 2\mu)\boldsymbol{\nabla}(\boldsymbol{\nabla} \cdot \mathbf{u}) - \mu\boldsymbol{\nabla} \times \boldsymbol{\nabla} \times \mathbf{u}. \tag{3}$$

We choose to represent $\mathbf{u}$ by (Backus, 1967)

$$\mathbf{u} = \widehat{\mathbf{r}}U + \boldsymbol{\nabla}_1 V - \widehat{\mathbf{r}} \times \boldsymbol{\nabla}_1 W \tag{4}$$

where U, V, and W are scalar fields and $\boldsymbol{\nabla}_1$ is defined by

$$\boldsymbol{\nabla}_1 = \widehat{\theta}\partial_\theta + \widehat{\phi}(\sin\theta)^{-1}\partial\phi. \tag{5}$$

$\widehat{\mathbf{r}}$ is a unit vector directed away from the origin, θ and ϕ are the colatitude and longitude, and $\widehat{\theta}$ and $\widehat{\phi}$ are their respective unit vectors. $\boldsymbol{\nabla}_1$ is the gradient operator on the surface of a sphere of unit radius. It is related to the three-dimensional gradient operator by

$$\boldsymbol{\nabla} = \widehat{\mathbf{r}}\partial_r - r^{-1}\boldsymbol{\nabla}_1. \tag{6}$$

After some algebra, we can show (Backus, 1967) that

$$\begin{aligned}\boldsymbol{\nabla}(\boldsymbol{\nabla}\cdot\mathbf{u}) = {} & \widehat{\mathbf{r}}\partial_r\left\{\left(\partial_r+\frac{2}{r}\right)U + r^{-1}\nabla_1^2 V\right\} \\ & + \boldsymbol{\nabla}_1\left\{\left(r^{-1}\partial_r+\frac{2}{r^2}\right)U + r^{-2}\nabla_1^2 V\right\},\end{aligned} \tag{7}$$

and

$$\begin{aligned}\boldsymbol{\nabla}\times\boldsymbol{\nabla}\times\mathbf{u} = {} & \widehat{\mathbf{r}}\left\{r^{-2}\partial_r\left(r\nabla_1^2 V\right) - r^{-2}\nabla_1^2 U\right\} \\ & + \boldsymbol{\nabla}_1\left\{r^{-1}\partial_r U - r^{-1}\partial_r^2(rV)\right\} \\ & + \widehat{\mathbf{r}}\times\boldsymbol{\nabla}_1\left\{r^{-2}\nabla_1^2 W + r^{-1}\partial_r^2(rW)\right\}.\end{aligned} \tag{8}$$

We insert equations 4, 7, and 8 into equation 3. We now appeal to the uniqueness of the representation 4 (Backus, 1967) to yield the three coupled partial differential equations.

$$\begin{aligned}\rho\partial_t^2 U = {} & (\lambda+2\mu)\,\partial_r\left\{\left(\partial_r+\frac{2}{r}\right)U + r^{-1}\nabla_1^2 V\right\} \\ & - \frac{\mu}{r^2}\left\{\partial_r\left(r\nabla_1^2 V\right) - \nabla_1^2 U\right\},\end{aligned} \tag{9a}$$

$$\begin{aligned}\rho\partial_t^2 V = {} & (\lambda+2\mu)\left\{\left(r^{-1}\partial_r+\frac{2}{r^2}\right)U + r^{-2}\nabla_1^2 V\right\} \\ & - \frac{\mu}{r}\left\{\partial_r U - \partial_r^2(rV)\right\},\end{aligned} \tag{9b}$$

and

$$\rho\partial_t^2 W = \frac{\mu}{r}\left\{\partial_r^2(rW) + r^{-1}\nabla_1^2 W\right\}. \tag{9c}$$

We note that both V and W may be augmented by any constant without affecting $\mathbf{u}$ (see equation 4). Therefore, we may expect these two scalar fields to be determined only to within an additive constant. We also note that equations 9a and 9b both involve U and V but not W, while equation 9c involves W but neither U nor V.

The manner in which one elects to solve equations 9a, 9b and 9c (plus whatever boundary conditions appertain) depends upon the intended application of the solution.

For our purposes, we wish to find a set of linearly independent vector fields, each of which satisfies equation 3. If the set is complete, all possible solutions to equation 3 may then be expressed as some linear combination of the members of the set, the coefficients used in the expansion being determined by boundary and initial conditions.

In pursuit of this, we Fourier transform equations 9a–9c, going from time t to angular frequency ω. We do not introduce a distinct symbol for Fourier transforms since it will be clear from the context whether a symbol refers to the transformed or untransformed variable. The result of Fourier transformation is to replace ∂_t^2 by $-\omega^2$.

To transform the resultant trio of equations from partial to ordinary differential equations we introduce a surface spherical harmonic expansion of U, V and W. For $l \geq 0$ and $-l \leq m \leq l$, we define (Hill, 1954)

$$Y_l^m(\theta, \phi) = (-1)^m \left[\frac{2l+1}{4\pi} \frac{(l-|m|)!}{(l+|m|)!} \right]^{\frac{1}{2}} P_l^m(\cos\theta) e^{im\phi} \tag{10}$$

where P_l^m is the Associated Legendre Function given by

$$P_l^m(x) = \frac{(1-x^2)^{\frac{|m|}{2}}}{2^l\, l!} \, \partial_x^{l+|m|} (x^2-1)^l. \tag{11}$$

If S_1 is the surface of a sphere of unit radius centered on the origin, the Y_l^m are orthonormal in the sense

$$\int_{S_1} Y_l^m(\theta, \phi)\, Y_\lambda^\mu(\theta, \phi)^\dagger \sin\theta \, d\theta \, d\phi = \delta_{l\lambda} \delta_{m\mu} \tag{12}$$

where the bar indicates complex conjugation and δ_{ij} is the Kronecker delta.

The $Y_l^m(\theta, \phi)$ form a complete set and, if we assume that U, V and W are sufficiently regular, we may expand them as

$$U(r, \theta, \phi, \omega) = \sum_{l=0}^{\infty} \sum_{m=-l}^{l} U_l^m(r, \omega)\, Y_l^m(\theta, \phi), \tag{13a}$$

$$V(r,\theta,\phi,\omega) = \sum_{l=1}^{\infty} \sum_{m=-l}^{l} V_l^m(r,\omega)\, Y_l^m(\theta,\phi), \tag{13b}$$

and

$$W(r,\theta,\phi,\omega) = \sum_{l=1}^{\infty} \sum_{m=-l}^{l} W_l^m(r,\omega)\, Y_l^m(\theta,\phi). \tag{13c}$$

The $l = 0$ terms have been omitted from equations 13b and 13c since inspection of equation 4 reveals that these terms do not contribute to the displacement field.

We now insert equations 13a–13c into the transformed equations 9a–9c, and make use of the relation

$$\nabla_1^2 Y_l^m = -l(l+1) Y_l^m. \tag{14}$$

The resultant expressions are then multiplied by a particular Y_l^m and integrated over the surface of a sphere of radius r. Application of equation 12 leads immediately to the set of coupled *ordinary* differential equations:

$$\begin{aligned} -\rho\omega^2 U_l^m = (\lambda+2\mu)\partial_r &\left\{ \left(\partial_r + \frac{2}{r}\right) U_l^m - \frac{l(l+1)}{r} V_l^m \right\} \\ &+ \frac{\mu}{r^2}\left\{ l(l+1)\partial_r (r V_l^m) - l(l+1) U_l^m \right\} \end{aligned} \tag{15a}$$

$$\begin{aligned} -\rho\omega^2 V_l^m = (\lambda+2\mu) &\left\{ \left(r\partial_r + \frac{2}{r^2}\right) U_l^m - \frac{l(l+1)}{r^2} V_l^m \right\} \\ &- \frac{\mu}{r}\left\{ \partial_r U_l^m - \partial_r^2 \left(r V_l^m\right) \right\} \end{aligned} \tag{15b}$$

and

$$-\rho\omega^2 W_l^m = \frac{\mu}{r}\left\{ \partial_r^2 \left(r W_l^m\right) - \frac{l(l+1)}{r} W_l^m \right\}. \tag{15c}$$

We note that none of equations 15a–15c explicitly involves m.

The set 15a–15c can be solved by any of several standard techniques. The method used here is detailed in Appendix A. The results are, for $l > 0$,

$$\left\{ \begin{array}{c} U_l^m \\ V_l^m \end{array} \right\} = \left\{ \begin{array}{cccc} \partial_r j_l(kr) & \dfrac{l(l+1)}{r} j_l(\gamma r) & \partial_r y_l(kr) & \dfrac{l(l+1)}{r} y_l(\gamma r) \\ \dfrac{j_l(kr)}{r} & r^{-1}\partial_r\left[r j_l(\gamma r)\right] & \dfrac{y_l(kr)}{r} & r^{-1}\partial_r\left[r j_l(\gamma r)\right] \end{array} \right\} \left\{ \begin{array}{c} A_l^m \\ B_l^m \\ C_l^m \\ D_l^m \end{array} \right\} \tag{16}$$

and for $l = 0$

$$U_0^0 = \{\partial_r j_0(kr)\, \partial_r y_0(kr)\} \left\{ \begin{array}{c} A_0^0 \\ C_0^0 \end{array} \right\} \tag{17a}$$

$$V_0^0 = 0; \tag{17b}$$

$$W_l^m = \{r j_l(\gamma r)\, r y_l(\gamma r)\} \left\{ \begin{array}{c} E_l^m \\ F_l^m \end{array} \right\} \qquad \text{for } l > 0; \tag{18a}$$

$$W_0^0 = 0; \tag{18b}$$

where

$$k = \frac{\omega}{\sqrt{\dfrac{(\lambda + 2\mu)}{\rho}}} = \frac{\omega}{V_p}, \tag{19}$$

and

$$\gamma = \frac{\omega}{\sqrt{\dfrac{\mu}{\rho}}} = \frac{\omega}{V_s}. \tag{20}$$

V_p and V_s are, respectively, the velocities of compressional and shear waves in the medium. The functions $j_l(x)$ and $y_l(x)$ are spherical Bessel functions defined by

$$j_l(x) = \sqrt{\frac{\pi}{2x}}\, J_{l+\frac{1}{2}}(x) \tag{21}$$

and

$$y_l(x) = \sqrt{\frac{\pi}{2x}}\, Y_{l+\frac{1}{2}}(x) \tag{22}$$

where J_l and Y_l are conventional cylindrical Bessel functions.

We note that the functional form of the solutions 16–18 is independent of m. The degeneracy of this index, which will persist to the case of a layered sphere, is a direct result of spherical symmetry. Any linear combination of surface spherical harmonics of order l,

$$H_l = \sum_{m=-l}^{l} \alpha_l^m Y_l^m \tag{23}$$

is itself a surface spherical harmonic of order l and satisfies equation 14.

3 Free Oscillations of a Layered Elastic Sphere

We consider a sphere divided into N concentric spherical shells. We number the shells from the center outwards and let r_i be the outermost radius of the i^{th} shell. Then $r_{\scriptscriptstyle N}$ is the radius of the sphere. Let r_0 equal zero. We suppose that the i^{th} shell is composed of an elastic, homogeneous, isotropic medium of density ρ_i and having Lamé parameters λ_i and μ_i.

We assume that the surface $r = r_{\scriptscriptstyle N}$ is free from all tractions, and that no body forces (such as gravitation) are present. We wish to know for what angular frequencies ω there exists a non-trivial displacement $\mathbf{u}(\mathbf{r})e^{i\omega t}$, such that the surface is free of traction and all internal boundary conditions (discussed below) are fulfilled. We shall label such angular frequencies *eigenfrequencies* and their associated displacements *eigenfunctions*. We refer to such traction-free motions as *free oscillations*.

Let $\mathbf{u}^{(i)}(\mathbf{r})e^{i\omega t}$ be the displacement field in the i^{th} layer. From the displacement, we can compute a stress tensor $\mathbb{T}^{(i)}$ by equation 1. Equation 2, namely

$$\rho\partial_t^2\mathbf{u} = \boldsymbol{\nabla}\cdot\mathbb{T} \tag{2}$$

must hold everywhere in the medium, since it expresses only the conservation of linear momentum and is not dependent upon such assumptions as isotropy, homogeneity, *etc.* In particular, equation 2 is valid in a small "Gaussian pillbox" which encompasses a portion of the surface $r = r_i$, the boundary between the i^{th} and $(i+1)^{\text{th}}$ shells. Let v denote the volume enclosed between the radii $r_i - \delta r$ and $r_i + \delta r$ and by some range of the coordinates θ and ϕ. Then

$$\int_v \rho\partial_t^2\mathbf{u}\,dv = \int_v \boldsymbol{\nabla}\cdot\mathbb{T}\,dv. \tag{24}$$

If Σ is the surface of v, Gauss's theorem leads to

$$\int_v \rho\partial_t^2\mathbf{u}\,dv = \int_\Sigma \mathbb{T}\cdot\widehat{\mathbf{n}}\,d\sigma$$

where $\widehat{\mathbf{n}}$ is the unit outward normal on Σ. If we let δr go to zero, then the volume of v also vanishes and, if $\rho\partial_t^2\mathbf{u}$ remains bounded, the left-hand integral goes to zero. The right-hand side becomes

$$\int_\Sigma \left\{\mathbb{T}^{(i+1)} - \mathbb{T}^{(i-1)}\right\}\cdot\widehat{\mathbf{r}}\,d\sigma = 0 \qquad \text{at } r = r_i. \tag{25}$$

Since this result is independent of the details of the shape of Σ we conclude that the quantity $\mathbb{T}\cdot\widehat{\mathbf{r}}$ must be everywhere continuous, and in particular across boundaries.

To condition 25 we add one expressing our intuition of the behavior of elastic materials. If both the i^{th} and $(i+1)^{\text{th}}$ shells are solid, we require that the displacement $\mathbf{u}$ be continuous. We refer to interfaces at which this is true as being "welded." If, however, one or both shells are fluid (that is, $\mu = 0$), we require only the radial component of displacement to be continuous. In the latter case, we allow the boundary to slip laterally but in neither case do we allow holes to open or matter to interpenetrate itself.

The quantity $\mathbb{T} \cdot \widehat{\mathbf{r}}$ is a vector and is the traction (force) acting on a surface with normal $\widehat{\mathbf{r}}$. In a fashion identical to equation 4, we may represent it as

$$\mathbb{T} \cdot \widehat{\mathbf{r}} = \widehat{\mathbf{r}} P + \boldsymbol{\nabla}_1 Q - \widehat{\mathbf{r}} \times \boldsymbol{\nabla}_1 R, \tag{26}$$

where P, Q and R are scalar fields. Equation 25 states that P, Q and R are continuous across an interface. The stress-displacement relations, equation 1, enable us to relate P, Q and R to U, V and W, the scalar representatives for $\mathbf{u}$. These relations, which are derived in Appendix B, are

$$P = (\lambda + 2\mu)\partial_r U + \frac{2\lambda}{r} U + \frac{\lambda}{r} \nabla_1^2 V, \tag{27a}$$

$$Q = \mu \left\{ \frac{U}{r} + r\partial_r \left(\frac{V}{r} \right) \right\}, \tag{27b}$$

and

$$R = \mu r \partial_r \left(\frac{W}{r} \right). \tag{27c}$$

The import of the boundary conditions, then, is that P, Q, R and U are continuous everywhere and V and W are continuous in solid domains.

We now have six scalar fields to contend with. However, an examination of equations 16, 17, 18 and 27 indicates that we can group them into two sets, one consisting of U, V, P and Q, and one consisting of W and R. These two sets are completely independent; they do not interact in any way. We may, without loss of generality, treat them separately.

The set (U, V, P, Q) is the set of *spheroidal* variables. The displacements described by this set give rise to both compressional and shear strain, and are interference products of compressional and vertically polarized shear waves. Rayleigh surface waves are one product of this class of motion.

The set (W, R) is the set of *toroidal* variables. The displacements described by this set are orthogonal to $\widehat{\mathbf{r}}$ and produce only shear strain. They are the interference products of horizontally polarized shear waves. Love surface waves are associated with this set.

From this point forward we will discuss only spheroidal types of motion. A similar development for toroidal oscillations can be easily formulated since the toroidal problem is substantially simpler.

For any specified angular frequency of oscillation ω, the set (U, V, P, Q) can be expanded in terms of spherical harmonics as

$$U(r,\theta,\phi,\omega) = \sum_{l=0}^{\infty} \sum_{m=-l}^{l} U_l^m(r,\omega)\, Y_l^m(\theta,\phi) \tag{13a}$$

$$V(r,\theta,\phi,\omega) = \sum_{l=1}^{\infty} \sum_{m=-l}^{l} V_l^m(r,\omega)\, Y_l^m(\theta,\phi) \tag{13b}$$

$$P(r,\theta,\phi,\omega) = \sum_{l=0}^{\infty} \sum_{m=-l}^{l} P_l^m(r,\omega)\, Y_l^m(\theta,\phi) \tag{28a}$$

$$Q(r,\theta,\phi,\omega) = \sum_{l=1}^{\infty} \sum_{m=-l}^{l} Q_l^m(r,\omega)\, Y_l^m(\theta,\phi). \tag{28b}$$

The U_l^m and V_l^m are given, in terms of a set of coefficients, by the analytic solutions 16 and 17. P_l^m and Q_l^m are then given by equation 27. Our problem is to determine those frequencies, ω, for which we can construct U, V, P and Q for each layer, such that all boundary and interface conditions are met.

Because the Y_l^m are an orthogonal set, we may consider the above problem separately for each Y_l^m. That is, given

$$U(r,\theta,\phi,\omega) = U_l^m(r,\omega)\, Y_l^m(\theta,\phi), \tag{29}$$

etc., for what angular frequencies ω can we satisfy all internal and external boundary conditions? Since m, as discussed earlier, is a degenerate index, we can simplify equation 29 to

$$U(r,\theta,\phi,\omega) = U_l(r,\omega)\, H_l(\theta,\phi) \tag{30a}$$

$$V(r,\theta,\phi,\omega) = V_l(r,\omega)\, H_l(\theta,\phi) \tag{30b}$$

$$P(r,\theta,\phi,\omega) = P_l(r,\omega)\, H_l(\theta,\phi) \tag{30c}$$

and

$$Q(r,\theta,\phi,\omega) = Q_l(r,\omega)\, H_l(\theta,\phi) \tag{30d}$$

where H_l is given by equation 23 and is some spherical harmonic of degree l. The details of H_l are of no particular interest at present since the eigenfrequencies and the form of $U_l, \ldots, Q_l$ remain fixed no matter what H_l we choose.

Our problem now is to find the eigenfrequencies associated with spherical harmonics of degree l. If we wish to know all eigenfrequencies, we must repeat this procedure for each of $l = 0, 1, 2, \ldots$.

We will devise a constructive algorithm which will enable us, for a given angular frequency ω, to construct a solution from the center outward which meets all boundary conditions save one. If the last condition is met, ω is an eigenfrequency. The method we present here is one application of the use of propagator matrices. The general method is discussed by Gilbert and Backus (Gilbert & Backus, 1966). Seismological applications are numerous (see, for example, (Harkrider, 1964), (Ben-Menahem, 1964) and (Anderson, 1966)).

We consider equation 16, which expresses U_l and V_l as a linear combination of four independent functions of radius. Equation 27 allows us to extend equation 16 to

$$\left\{\begin{array}{c} U_l^i \\ V_l^i \\ P_l^i \\ Q_l^i \end{array}\right\} = \mathbb{H}_l^i \left\{\begin{array}{c} A_l^i \\ B_l^i \\ C_l^i \\ D_l^i \end{array}\right\} \tag{31}$$

where $i = 1, \ldots, N$ designates the layer to which the solution is appropriate. $\mathbb{H}_l^i$ is a 4×4 matrix constructed from

$$h_{3j} = (\lambda + 2\mu)\partial_r h_{1j} + \frac{2\lambda}{r} h_{1j} - \lambda \frac{l(l+1)}{r} h_{2j}, \tag{32a}$$

and

$$h_{4j} = \mu \left\{ r^{-1} h_{1j} + r\partial_r \left(r^{-1} h_{2j} \right) \right\} \tag{32b}$$

and the first two rows of $\mathbb{H}_l^i$ are taken from equation 16. The set $\{A_l^i, \ldots, D_l^i\}$ are constants. We omit the θ and ϕ terms for convenience.

We rewrite equation 31 as

$$\mathbf{S}^i(r) = \mathbb{H}^i(r) \cdot \mathbf{C}^i \tag{33}$$

where we have omitted the subscript l. The vector $\mathbf{S}^i(r)$ includes both the stress and displacement terms.

We will now proceed to construct a solution satisfying all internal boundary conditions. In region 1 which includes the point $r = 0$ we can *a priori* eliminate those solutions which go as $y_l(kr)$ and $y_l(\gamma r)$. Therefore, $\mathbf{C}^1$ has the form

$$\mathbf{C}^1 = \left\{ \begin{array}{c} A^1 \\ B^1 \\ 0 \\ 0 \end{array} \right\} = A^1\widehat{\mathbf{e}}_1 + B^1\widehat{\mathbf{e}}_2 \tag{34}$$

where $\widehat{\mathbf{e}}_1$ and $\widehat{\mathbf{e}}_2$ are Euclidean four-dimensional unit coordinate vectors directed along the first and second coordinate axes. In the first region, then, we have

$$\mathbf{S}^1(r) = \mathbb{H}^1(r) \cdot \left\{A^1\widehat{\mathbf{e}}_1 + B^1\widehat{\mathbf{e}}_2\right\}. \tag{35}$$

In the second region, we have

$$\mathbf{S}^2(r) = \mathbb{H}^2(r) \cdot \mathbf{C}^2. \tag{36}$$

Assuming both regions to be solid, the boundary conditions require that

$$\mathbf{S}^2(r_1) = \mathbf{S}^1(r_1), \tag{37}$$

or

$$\mathbb{H}^2(r_1) \cdot \mathbf{C}^2 = \mathbb{H}^1(r_1) \cdot \left\{A^1\widehat{\mathbf{e}}_1 + B^1\widehat{\mathbf{e}}_2\right\}. \tag{38}$$

Because the solutions composing the columns of $\mathbb{H}$ are linearly independent, matrix theory guarantees that $\mathbb{H}$ is nonsingular. Therefore, we may express $\mathbf{C}^2$ as

$$\mathbf{C}^2 = \left[\mathbb{H}^2(r_1)\right]^{-1} \cdot \mathbb{H}^1(r_1) \cdot \left\{A^1\widehat{\mathbf{e}}_1 + B^1\widehat{\mathbf{e}}_2\right\}. \tag{39}$$

An alternative form for equation 39 is

$$\mathbf{C}^2 = A^1\xi^2 + B^1\zeta^2 \tag{40}$$

where

$$\xi^2 = \left[\mathbb{H}^2(r_1)\right]^{-1} \cdot \mathbb{H}^1(r_1) \cdot \widehat{\mathbf{e}}_1 \tag{41}$$

$$\zeta^2 = \left[\mathbb{H}^2(r_1)\right]^{-1} \cdot \mathbb{H}^1(r_1) \cdot \widehat{\mathbf{e}}_2 \tag{42}$$

Equations 40, 41 and 42 suffice to specify $\mathbf{S}^2(r)$. By a similar procedure, we can extend the solution from the i^{th} to the $(i+1)^{\text{th}}$ shell. The appropriate relations are

$$\mathbf{S}^{i+1}(r) = \mathbb{H}^{i+1}(r) \cdot \mathbf{C}^{i+1} \tag{43}$$

$$\mathbf{C}^{i+1} = A^1\xi^{i+1} + B^1\zeta^{i+1} \tag{44}$$

$$\xi^{i+1} = \left[\mathbb{H}^{i+1}(r)\right]^{-1} \cdot \mathbb{H}^i(r) \cdot \xi^i \tag{45}$$

$$\zeta^{i+1} = \left[\mathbb{H}^{i+1}(r)\right]^{-1} \cdot \mathbb{H}^i(r) \cdot \zeta^i. \tag{46}$$

In fact, either of ξ^{i+1} or ζ^{i+1} can be computed alone by starting with equation 41 or 42 and simply applying equation 45 or 46 as many times as is necessary.

We suppose now that we have computed ξ^N and ζ^N where N is the number of shells. The solution in this shell is given by

$$\mathbf{S}^N(r) = \mathbb{H}^N(r) \cdot \left\{A^1\xi^N + B^1\zeta^N\right\}. \tag{47}$$

We note that both the solution associated with ξ^N [*i.e.*, $\mathbf{S}^N(r)$ when $B^1 = 0$] and the solution associated with ζ^N separately satisfy all of the internal boundary conditions. If ω is an eigenfrequency, we will be able to find some A^1 and B^1, not both zero, such that the last two components of $\mathbf{S}^N(r_N)$ are zero.

A straightforward way to do this is to evaluate

$$^{(a)}\mathbf{S}^N = \mathbb{H}^N(r_N) \cdot \xi^N, \tag{48a}$$

and

$$^{(b)}\mathbf{S}^N = \mathbb{H}^N(r_{_N}) \cdot \zeta^N. \tag{48b}$$

If $\mathbf{S}_3^N(r_{_N})$, *i.e.* P, must vanish, A^1 and B^1 must satisfy

$$A^1\left({}^aS_3^N\right) = -B^1\left({}^bS_3^N\right). \tag{49}$$

We may, without loss of generality, impose a normalization such as

$$\left(A^1\right)^2 + \left(B^1\right)^2 = 1, \tag{50}$$

which, with equation 49, allows us to compute A^1 and B^1. Using A^1 and B^1, we then compute $S_4^N(r_{_N})$, *i.e.* Q, and examine it to see if it vanishes. If it does, ω is an eigenfrequency; if it does not, ω is not an eigenfrequency.

If ω is an eigenfrequency then we may use the values of A^1 and B^1 in equations 43 and 44 to compute the eigenfunction $\mathbf{S}^i(r)$ at any radius in the system. We recall that $\mathbf{S}^i(r)$ must be multiplied by some spherical harmonic of degree l and the factor $e^{i\omega t}$ to obtain the full solution,

$$\mathbf{S}_l^i(r,\theta,\phi,t) = \mathbf{S}_l^i(r)H_l(\theta,\phi)e^{i\omega t}$$

where we have reinstated the subscript l. We emphasize again that the precise nature of H_l depends upon other considerations and is not relevant here.

This method requires modification when either $l = 0$, or $l \neq 0$ but one or more shells have a vanishing shear modulus. We will briefly outline the form these modifications take.

When $l = 0$, B^1 vanishes identically and only one solution is propagated. The matrix $\mathbb{H}_l^i$ is collapsed to a 2×2 matrix by eliminating those solutions with arguments

γr. V and Q both vanish and the only condition at $r = r_N$ is that P vanish. A^1 becomes merely a scale factor and may be taken as equal to unity.

In a fluid region, Q vanishes identically. Across a solid/fluid or fluid/fluid interface V may be discontinuous and Q is continuous and zero. If we are propagating upward through a solid and encounter a fluid, we must combine the ξ and ζ solutions to yield $Q = 0$ at the interface. This requirement determines A^1 and B^1 and, therefore, $\mathbf{C}^i$ for all shells up to, and including, the fluid region.

Consequently, in a fluid region we have only one solution. In crossing from a fluid to a solid region, we must start an additional new solution having some non-zero V, but for which U, P and Q vanish. We may always find some ζ which yields this result.

For a given l, we shall arrange the frequencies of free oscillation in ascending order, as ${}_0\omega_l, {}_1\omega_l, \ldots$ and the four-vector of displacement and stress by ${}_0\mathbf{S}_l, {}_1\mathbf{S}_l, \ldots,$ *etc.* The "lowest" mode, for a given l, is referred to as the "fundamental" mode and the remainder as "overtones."

Each mode of order l represents, in fact, a space of modes of dimension $2l+1$ (the number of possible values for m between $-l$ and $+l$). Each member of this space has the same eigenvalue and depends functionally upon radius in the same way, but is associated with a different surface spherical harmonic of order l. The entire set of modes for a given layered sphere consists of the doubly infinite sets ($0 \le n \le \infty$ and $0 \le l \le \infty$) of $2l+1$ degenerate spheroidal and toroidal modes.

This set is complete (Backus, 1967) and therefore any elastic motion, consistent with the foregoing boundary conditions, which the system may undergo can be described as a sum, in the time domain, of members of this set. A discussion of the asymptotic relations between modes and "waves" is given by Ben-Menahem (Ben-Menahem, 1964).

As an example of this we note that

$$Y_l^l(\theta,\phi) = (-1)^l \sqrt{\frac{2l+1}{4\pi(2l)!}}\,\frac{(\sin\theta)^l}{2^l}\,e^{il\phi} \tag{51}$$

as can be seen from equations 10 and 11. Y_l^l describes motion which is closely confined to the equator ($\theta = \pi/2$) and which behaves as waves traveling circumferentially about the equatorial zone. The change of phase, per unit of distance traveled in the $\widehat{\phi}$ direction, is l/a and is therefore the mode's surface wave number. For large values of ω, we may, roughly, expect that the quantity

$$U^* = a\,\frac{\partial\omega}{\partial l} \tag{52}$$

represents a group velocity and

$$C^* = \frac{a\omega}{l} \tag{53}$$

represents a phase velocity.

4 Energy Densities and Rayleigh's Principle

The n^{th} overtone of the spheroidal mode of degree l has displacements ${}_n\mathbf{u}_l$, given by

$${}_n\mathbf{u}_l = \widehat{\mathbf{r}}\,{}_nU_l(r)H_l(\theta,\phi) + {}_nV_l(r)\boldsymbol{\nabla}_1 H_l(\theta,\phi) \tag{54}$$

where H_l is some surface harmonic of degree l. The left subscript, n, denotes the overtone to which U and V are appropriate.

The total kinetic energy of motion, averaged over one cycle, is given by

$$E_K = \frac{1}{2}\,{}_n\omega_l^2 \int_V \rho\left({}_n\mathbf{u}_l\right)\cdot\left({}_n\mathbf{u}_l{}^{\dagger}\right)\,dv. \tag{55}$$

Using the results of Backus (Backus, 1967), we can show

$$E_K = \frac{1}{2}\, {}_n\omega_l^2 \int_0^{r_n} \rho r^2 \left[{}_nU_l^2 + l(l+1)\, {}_nV_l^2\right]\, dr \tag{56}$$

when H_l is normalized such that

$$\int_{S_1} H_l\, H_l^\dagger \sin\theta\, d\theta\, d\phi = 1 \tag{57}$$

(see equation 12).

The total elastic energy is given by

$$E_\sigma = \frac{1}{2} \int_V \mathrm{tr}\,(\mathbb{T} \cdot \epsilon)\; dV \tag{58}$$

where "tr" indicates the trace operator, $\mathbb{T}$ is, as before, the elastic stress tensor, and ϵ is the (infinitesimal) strain tensor defined by

$$\epsilon = \frac{1}{2}\left\{\boldsymbol{\nabla}\mathbf{u} + \mathbf{u}\boldsymbol{\nabla}\right\}. \tag{59}$$

After some algebra, we can show

$$\begin{aligned} E_\sigma = \frac{1}{2}\int_0^{r_N} \Big\{ &\lambda\Big[r\partial_r U + 2U - l(l+1)V\Big]^2 \\ &+ \mu\Big[2\,(r\partial_r U)^2 + l(l+1)(U + r\partial_r V - V)^2 \\ &+ [2U - l(l+1)V]^2 + (l-1)l(l+1)(l+2)V^2\Big]\Big\}\, dr \end{aligned} \tag{60}$$

where, for simplicity, we have dropped the subscripts n and l.

When ${}_n\mathbf{u}_l$ is an eigenfunction of the system we are interested in, and ${}_n\omega_l^2$ is its associated eigenvalue, we have

$$E_K = E_\sigma. \tag{61}$$

If we define

$$K = \left[U^2 + l(l+1)V^2\right] r^2, \tag{62}$$

$$L = \left\{r\partial_r U + 2U - l(l+1)V\right\}^2, \tag{63}$$

and

$$\begin{aligned} M = {} & 2(r\partial_r U)^2 + l(l+1)(U + r\partial_r V - V)^2 \\ & + [2U - l(l+1)V]^2 + (l-1)l(l+1)(l+2)V^2 \end{aligned} \tag{64}$$

we may rewrite equation 61 as

$${}_n\omega_l^2 = \frac{\int_0^{r_N} (\lambda L + \mu M)\ dr}{\int_0^{r_N} \rho K\, dr}. \tag{65}$$

As first pointed out by Rayleigh (Rayleigh, 1945) and discussed by Backus and Gilbert (Backus & Gilbert, 1967), the functional ${}_n\omega_l^2({}_n\mathbf{u}_l)$, defined by equations 62–65, is stationary with respect to small variations in ${}_n\mathbf{u}_l$ if ${}_n\mathbf{u}_l$ is an eigenfunction associated with ${}_n\omega_l^2$. As a consequence of this, we may use equation 65 to relate, to first order, small changes in λ, μ and ρ to small changes in ${}_n\omega_l^2$. The result is

$$\delta\left({}_n\omega_l^2\right) = \frac{\int_0^{r_N} (\delta\lambda L + \delta\mu M - \delta\rho\omega^2 K)\ dr}{\int_0^{r_N} \rho K\, dr} \tag{66}$$

where, clearly,

$$\delta\left({}_n\omega_l^2\right) = 2\,{}_n\omega_l \delta\left({}_n\omega_l\right).$$

The "partial derivatives" of ${}_n\omega_l$ with respect to λ, μ and ρ may be converted to those with respect to V_p, V_s and ρ by application of

$$\left(\frac{\partial\mu}{\partial\rho}\right)_{V_p,V_s} = V_s^2 \tag{67a}$$

$$\left(\frac{\partial\lambda}{\partial\rho}\right)_{V_p,V_s} = V_p^2 - 2V_s^2 \tag{67b}$$

$$\left(\frac{\partial\mu}{\partial V_s}\right)_{V_p,\rho} = 2\rho V_s \tag{67c}$$

$$\left(\frac{\partial\lambda}{\partial V_s}\right)_{V_p,\rho} = -4\rho V_s \tag{67d}$$

$$\left(\frac{\partial\mu}{\partial V_p}\right)_{V_s,\rho} = 0 \tag{67e}$$

and

$$\left(\frac{\partial\lambda}{\partial V_p}\right)_{V_s,\rho} = 2V_p\rho. \tag{67f}$$

5 Effects of a Slight Anelasticity

We now suppose that the perturbations in λ and μ are purely imaginary:

$$\delta\lambda = i\omega\lambda' \tag{68a}$$

$$\delta\mu = i\omega\mu' \tag{68b}$$

where λ' and μ' are real. This is precisely equivalent to replacing λ by $\lambda + \lambda'\partial_t$ and μ by $\mu + \mu'\partial_t$ in equation 3. Then

$$\delta\left({}_n\omega_l^2\right) = \frac{i\,{}_n\omega_l \int_0^{r_N} \left(\lambda' L + \mu' M\right)\, dr}{\int_0^{r_N} \rho K\, dr} \tag{69}$$

to *first order* in λ' and μ'. Alternatively,

$$\delta\left({}_n\omega_l^2\right) = i\,{}_n\omega_l\,{}_nD_l \tag{70}$$

which serves to define ${}_nD_l$. Therefore

$$\delta\left({}_n\omega_l\right) = \frac{i}{2}\,{}_nD_l \tag{71}$$

and the lumped quality factor ${}_nQ_l$ is given by

$${}_nQ_l = \frac{{}_n\omega_l}{{}_nD_l}. \tag{72}$$

We define

$$Q_{V_p}^{-1} = \frac{\omega}{\lambda+2\mu}\left(\lambda'+2\mu'\right) \tag{73}$$

and

$$Q_{V_s}^{-1} = \frac{\omega}{\mu}\mu'. \tag{74}$$

These are, respectively, the inverse Q's of pure compressional and pure shear waves in a homogeneous, slightly lossy medium. From equations 73 and 74 it follows that

$$\mu' = \frac{\mu}{\omega}Q_{V_s}^{-1} \tag{75}$$

$$\lambda' = \left(\frac{\lambda+2\mu}{\omega}\right)Q_{V_p}^{-1} - 2\left(\frac{\mu}{\omega}\right)Q_{V_s}^{-1}. \tag{76}$$

Combining equations 69, 70, 72, 75 and 76, we have

$${}_nQ_l^{-1} = \frac{\frac{1}{{}_n\omega_l^2}\int_0^{r_N}\left[Q_{V_p}^{-1}\left(\lambda+2\mu\right)L + Q_{V_s}^{-1}\left(\mu M - 2\mu L\right)\right]\,dr}{\int_0^{r_N}\rho K\,dr}$$

or

$${}_nQ_l^{-1} = \frac{\int_0^{r_N}\left[Q_{V_p}^{-1}\left(\lambda+2\mu\right)L + Q_{V_s}^{-1}\mu\left(M - 2L\right)\right]\,dr}{2E_K}. \tag{77}$$

6 Results for a Layered System

The above expressions are all valid for a spherically symmetric body whose properties λ, μ and ρ are arbitrary (but reasonable) functions of position. For the sake of completeness, we give below specific expressions for a sphere composed of layered homogeneous shells.

For convenience, we suppose that we have always normalized ${}_n\mathbf{u}_l$ so that its kinetic energy is equal to $\frac{1}{2}\,{}_n\omega_l^2$. That is

$$\sum_{i=1}^{N} \rho_i \int_{r_{i-1}}^{r_i} K\,dr = 1. \tag{78}$$

Then the variation in ${}_n\omega_l$ due to perturbations in λ_i, μ_i and ρ_i for $i = 1, \ldots, N$ is

$$\delta({}_n\omega_l^2) = \sum_{i=1}^{N} \left[\sigma\lambda_i \int_{r_i-1}^{r_i} L\,dr + \delta\mu_i \int_{r_i-1}^{r_i} M\,dr - \delta\rho_i \int_{r_i-1}^{r_i} {}_n\omega_l^2 K\,dr \right]. \tag{79}$$

Equation 79 is an explicit representation of the perturbation in the $(n,l)^{\text{th}}$ squared eigenfrequency as a linear combination of perturbation in the layered sphere's parameters. Similarly, for $Q_{V_p}^{-1}$ and $Q_{V_s}^{-1}$, we have

$${}_nQ_l^{-1} = \frac{1}{{}_n\omega_l^2} \sum_{i=1}^{N} \left[Q_{V_p i}^{-1}(\lambda_i + 2\mu_i) \int_{r_{i-1}}^{r_i} L\,dr + Q_{V_s i}^{-1}\mu_i \int_{r_{i-1}}^{r_i} (M - 2L)\,dr \right]. \tag{80}$$

7 Forced Response of a Layered Elastic Sphere

We now consider the response of a layered elastic sphere, having a small anelasticity, to a specified driving force. This species of problem is classical (see (Rayleigh, 1945)) but we give our particular development here because, as a first approximation to our experiment, the specific theoretical results are quite helpful.

In the time domain, the appropriate field equation is

$$\rho \partial_t^2 \mathbf{u} = L\mathbf{u} + L' \partial_t \mathbf{u} + \vec{f} \tag{81}$$

where L is the elastic operator of equation 3, $\vec{f}$ is a spatial and temporal force distribution, and L' is an isotropic, viscous operator of the form

$$L' = (\lambda' + 2\mu')\boldsymbol{\nabla}\boldsymbol{\nabla}\cdot - \mu\boldsymbol{\nabla}\times\boldsymbol{\nabla}\times . \tag{82}$$

λ' and μ' are taken to be small and constant (see equation 68). Associated with equation 81 are the internal and external boundary conditions discussed earlier.

We Laplace transform equation 81 and assume (for convenience) that both $\mathbf{u}$ and $\partial_t \mathbf{u}$ vanish everywhere at time $t = 0$. Then equation 81 becomes, with p the transform variable,

$$\left(\rho p^2 - pL' - L\right)\mathbf{u} = \vec{f} \tag{83}$$

where $\mathbf{u}$ and $\vec{f}$ refer now to transformed variables. We shall expand $\mathbf{u}$ in the spheroidal eigenfunctions ${}_n\mathbf{u}_l$ as

$$\mathbf{u} = \sum {}_n a_l^j \, {}_n\mathbf{u}_l^j \tag{84}$$

and the sum is taken over all non-negative values of n and l, and $-l \le j \le l$. The ${}_n\mathbf{u}_l^j$ are orthogonal, as a result of the Hermitian nature of L and its boundary conditions. The set is, here, complete because the set of all free oscillations is complete (Backus, 1967) and we shall consider only a class of sources which cannot excite toroidal modes. We may further require the ${}_n\mathbf{u}_l^j$ to be orthonormal in the sense

$$\left(\rho \, {}_n\mathbf{u}_l^j, \, {}_m\mathbf{u}_k^s\right) = \int_v \rho \, {}_n\mathbf{u}_l^j \cdot \, {}_m\mathbf{u}_k^{s\,\dagger} \, dv = \delta_{nm}\delta_{lk}\delta_{js}. \tag{85}$$

If we insert the expansion 84 into equation 83, multiply on the left by ${}_m\mathbf{u}_k^s$, integrate, and use the result

$$L\,{}_n\mathbf{u}_l^j = -\rho\,{}_n\omega_l^2\,{}_n\mathbf{u}_l^j,$$

we find, after applying equation 85, that

$${}_m a_k^s\left[p^2 + {}_m\omega_k^2 - p\sum\left({}_m\mathbf{u}_k^s, L'\,{}_n\mathbf{u}_l^j\right)\right] = \left({}_m\mathbf{u}_k^s, \vec{f}\right).$$

Since L' is an isotropic operator, the inner product $({}_m\mathbf{u}_k^j, L'\,{}_n\mathbf{u}_l^s)$ will vanish for $k \neq l$ or $j \neq s$ as a result of the orthogonality of spherical harmonics. We do not know that this is true for $k = l$, $j = s$, $m \neq n$; that is, we do not know that anelasticity of this sort does not result in coupling between overtones with the same order l. For our purposes, however, we are interested in the effect of the anelastic term when one mode is strongly excited relative to other modes, *i.e.* near a resonance. This case is approximately the same as a response composed of a single mode, and we shall ignore possible overtone coupling. Following equation 70, we define the scalar

$${}_nD_l^j = -\left({}_n\mathbf{u}_l^j, L'\,{}_n\mathbf{u}_l^j\right). \tag{86}$$

Then we have

$${}_n a_l^j = \frac{\left({}_n\mathbf{u}_l^j, \vec{f}\right)}{p^2 + p\,{}_nD_l^j + {}_n\omega_l^2}. \tag{87}$$

(This does not constitute a redefinition of ${}_nD_l^j$. The quantity defined above is the same as that given by equations 69–70.)

We assume, for $\vec{f}(\mathbf{r}, t)$, the form

$$\vec{f}(\mathbf{r}, t) = \mathbf{r}\delta(\mathbf{r} - \mathbf{r}_s)\begin{cases}\sin(\kappa t) & t \geq 0\\ 0 & t \leq 0\end{cases} \tag{88}$$

where $\delta(\vec{x})$ is the three-dimensional Dirac delta function and $\mathbf{r}_s$ is the "source" location. Then equation 87 becomes

$$ {}_n a_l^j = \frac{\kappa \, {}_n U_l(r_s) \, Y_l^j(\theta_s, \phi_s)}{\left(p^2 + p \, {}_n D_l^j + {}_n\omega_l^2\right)\left(p^2 + \kappa^2\right)}. \tag{89} $$

${}_n U_l(r_s)$ is the value of the radial displacement component at r_s, the source radius. Since radial displacement vanishes identically for toroidal modes, a radial force source will not excite toroidal oscillations.

In order to compute the time-domain solution $\mathbf{u}(\mathbf{r}, t)$, we have to apply the inverse transform to equation 89 and use the resultant ${}_n a_l^j(t)$ in equation 84. The task is straightforward and we mention here only its salient, albeit predictable, features. ${}_n a_l^j$, as given in equation 89, has four singularities, one at each of $\pm i\kappa$, one at $-\frac{1}{2}\,{}_n D_l^j + i\sqrt{{}_n\omega_l^2 - \frac{1}{4}\,{}_n D_l^j}$ and one at $-\frac{1}{2}\,{}_n D_l^j - i\sqrt{{}_n\omega_l^2 - \frac{1}{4}\,{}_n D_l^j}$. The former two represent forced motion of the body at the frequency κ. Technically speaking, the forced component of motion exists because of the singularities in the transform of the source time function. Time functions such as delta, ramp and step functions whose transforms lack singularities do not give rise to such forced motion.

The second set of singularities represents free vibration at the body's various natural periods. These motions result from "turning on" the source at $t = 0$. They are damped exponentially and the farther in time one is from $t = 0$, the weaker these motions become.

For our purposes, we require only the forced motion and we will neglect the remaining poles. The result is

$$ a(t) = \frac{{}_n U_l(r_s) \, Y_l^j(\theta_s, \phi_s)}{(\omega^2 - \kappa^2)^2 + \kappa^2 D^2} \left[(\omega^2 - \kappa^2)\sin(\kappa t) + \kappa D \cos(\kappa t)\right] \tag{90} $$

where the subscripts have been deleted from a, ω and D for convenience.

We now suppose that the source is located at $\theta = 0$, $r = r_{_N}$ and that at $\theta = \pi$, $r = r_{_N}$ is emplaced a radial motion detector. For the latter location, equation 84 becomes

$$\sum {}_n a_l^0(t)(-1)^l \sqrt{\frac{2l+1}{4\pi}}\, {}_nU_l(r_{_N})$$

where the sum is taken only over n and l as a result of the source location.

The received power as a function of driving frequency κ is given by

$$R^2(\kappa) = \left(\sum \frac{{}_nA_l(-1)^l(\omega^2-\kappa^2)\omega^2}{(\omega^2-\kappa^2)^2+\kappa^2\omega^2/Q^2}\right)^2 + \left(\sum \frac{{}_nA_l(-1)^l\kappa\omega^3/Q}{(\omega^2-\kappa^2)^2+\kappa^2\omega/Q^2}\right)^2 \tag{91}$$

where

$${}_nA_l = \frac{{}_nU_l^2(r_{_N})\left(\dfrac{2l+1}{4\pi}\right)}{{}_n\omega_l^2}. \tag{92}$$

We have expressed $R^2(\kappa)$, the squared signal strength, in terms of the source factors ${}_nA_l$ and the lumped quality factors ${}_nQ_l$. If only a single mode need be considered, we have

$$R({}_n\omega_l) = {}_nA_l \cdot {}_nQ_l \tag{93}$$

which relates response maxima to both ${}_nA_l$ and ${}_nQ_l$.

It is straightforward to show that when only one mode is significant and

$$R^2(\kappa) = \frac{1}{2}R^2({}_n\omega_l) \tag{94}$$

then to first order in ${}_nQ_l^{-1}$, κ satisfies

$$\kappa = \frac{{}_n\omega_l \pm \frac{1}{2}\,{}_n\omega_l}{{}_nQ_l}. \tag{95}$$

Equation 95 is the classic relation between dissipation and peak width, and is useful only if ${}_nQ_l^{-1}$ is sufficiently small.

We have supposed above that the amplitude of $\vec{f}$ and the sensitivity of the radial displacement receiver were independent of frequency κ. If this is not so neither equation 93 nor equation 95 is necessarily correct. However, the half-power relation, equation 95, will generally be usable if source strength and receiver sensitivity do not vary appreciably over the range

$$\left[{}_n\omega_l\left(1-\tfrac{1}{2}\,{}_nQ_l^{-1}\right),{}_n\omega_l\left(1+\tfrac{1}{2}\,{}_nQ_l^{-1}\right)\right].$$

In anticipation of experiment, we mention that if the above influences are important or, as is more often the case, if the ${}_n\omega_l$ are sufficiently "dense" on the κ-axis, then neither equation 93 nor equation 95 will yield reliable measures of ${}_nQ_l^{-1}$. If this is the case, we will not be able to improve matters appreciably by making time domain measurements of the decay of a given mode. Irregularities in the "forced" spectrum will appear in the latter as distortions of a mode's exponential decay envelope.

We wish to make one further point, regarding restrictions on the nature of the dissipative mechanism, equation 82. Suppose that the time domain stress-strain relation is expressible as

$$\mathbb{T}=\mathbb{T}^e+\int_0^t \mathbb{C}(t-\tau):\partial_\tau\epsilon(\tau)\,d\tau, \tag{96}$$

where $\mathbb{T}^e$ is the elastic stress defined in equation 1, $\mathbb{C}$ is a fourth order tensor function of the time "lag," $t-\tau$, and $\epsilon(\tau)$ is the strain tensor,

$$\epsilon(\tau)=\frac{1}{2}\left(\boldsymbol{\nabla}\mathbf{u}+\mathbf{u}\boldsymbol{\nabla}\right). \tag{97}$$

We suppose both stress and strain to vanish for negative times. Laplace transforming equation 96 and supposing $\epsilon(0)$ to vanish gives

$$\mathbb{T}=\mathbb{T}^e+p\mathbb{C}(p):\epsilon(p). \tag{98}$$

When $\mathbb{C}$ is an isotropic tensor, the use of the stress defined in equation 98 in the transformed equations of motion (equation 2) will yield exactly operators of the form L and L' of equations 81 and 82. These differ from our usage only in the λ' and μ' may now depend functionally on p, the transform variable. The quantity ${}_nD_l$ defined by equation 86 or equations 69–70 would, in turn, depend upon p. If ${}_nD_l$ (or λ' and μ') does not vary appreciably over a frequency span of a "few peak-widths," the results derived above should be usefully accurate. (We must still have λ' and μ', or ${}_nD_l$, *small* since we have used a perturbation method to include attenuation.)

8 The Inverse Problem

In two of the preceding sections we developed the "forward" problem for a layered elastic sphere. The forward problem consists of the generation of the eigenvalue spectrum associated with a given model. In this section we consider the inverse problem of utilizing a measured eigenvalue spectrum (which will, inevitably, be incomplete) to infer the properties of the materials of which the sphere is composed.

Let $\mathfrak{M}$ be the space of all layered elastic spheres having N layers delimited by the points $\{r_0, r_1, \ldots, r_N\}$ where, as before, $r_0 = 0$ and r_N is the sphere's radius. Then all models in $\mathfrak{M}$ have a common geometry but differ in the elastic properties (including density) of their component shells. $\mathfrak{M}$, then, is a space of dimension $3N$ (since each shell has three distinct properties) and we may represent a given model by $\mathbf{m}$, a vector of dimension $3N$. We further limit $\mathfrak{M}$ by requiring that it encompass only physically realizable models. A model is said to be physically realizable if each shell's properties satisfy

$$\rho > 0, \tag{99a}$$

$$\mu \geq 0, \tag{99b}$$

and

$$\lambda \geq -\frac{2}{3}\mu, \tag{99c}$$

where both equalities 99b and 99c are not simultaneously true. Those two constraints merely express the condition that an elastic material be thermodynamically stable (Fung, 1965).

Let ${}_n\omega_l(\mathbf{m})$ be the n^{th} overtone of the spheroidal mode of degree l associated with the model $\mathbf{m}$. (Both n and l range over the non-negative integers.) We cannot express ${}_n\omega_l(\mathbf{m})$ in closed analytic form but we can, through techniques previously discussed, generate it numerically. We can now formulate the inverse problem in the following manner (Backus & Gilbert, 1967).

Let ${}_{n_i}\omega^0_{l_i}$, $i = 1, \ldots, K$ be observed resonant frequencies associated with particular modes of oscillation. We wish to determine a model $\mathbf{m}$, satisfying

$${}_{n_i}\omega_{l_i}(\mathbf{m}) = {}_{n_i}\omega^0_{l_i} \qquad i = 1, \ldots, K. \tag{100}$$

As Backus and Gilbert (Backus & Gilbert, 1967) have pointed out, we do not know, *a priori*, if the set of solutions to equations 100 is empty, has a single member, or is a subspace of $\mathfrak{M}$ with one or more dimensions.

We do not know a direct procedure for solving equation 100 for (one or more) $\mathbf{m}$. We resort here to iterative methods for generating successively improved approximations for $\mathbf{m}$. For convenience we rewrite equation 100 as

$$D_i(\mathbf{m}) = D_i^0 \qquad i = 1, \ldots, K \tag{101}$$

where the D_i^0 are *data* and the $D_i(\mathbf{m})$ are *data functions.* $D_i(\mathbf{m})$ is a scalar-valued function whose domain is the $3N$-dimensional vector space $\mathfrak{M}$ and whose value is the angular frequency of free oscillation of the n_i^{th} overtone of degree l_i. Let $\mathbf{m}^0$ be some model which we believe to lie near $\mathbf{m}$. We wish to find some perturbation, $\delta\mathbf{m}$, such that $\mathbf{m}^0 + \delta\mathbf{m}$ more nearly satisfies equation 101. We wish to have

$$D_i(\mathbf{m}^0 + \delta\mathbf{m}) = D_i^0 \qquad i = 1, \ldots, K. \tag{102}$$

Expanding $D_i(\mathbf{m})$ in a Taylor series gives

$$D_i(\mathbf{m}^0 + \delta\mathbf{m}) = D_i(\mathbf{m}^0) + \sum_{j=1}^{3N} \left[\frac{\partial D_i}{\partial m_j}\right]_{\mathbf{m}^0} \delta m_j + O(|\delta\mathbf{m}|^2) \qquad i = 1, \ldots, K. \tag{103}$$

Then, to first order in $|\delta\mathbf{m}|$, we wish $\delta\mathbf{m}$ to satisfy

$$\sum_{j=1}^{3N} \left[\frac{\partial D_i}{\partial m_j}\right]_{\mathbf{m}^0} \delta m_j = D_i^0 - D_i(\mathbf{m}^0) \qquad i = 1, \ldots, K. \tag{104}$$

If $|\delta\mathbf{m}|$ is sufficiently small we may expect that $\mathbf{m}^1 = \mathbf{m}^0 + \delta\mathbf{m}$ will more nearly satisfy equation 101 than $\mathbf{m}^0$ did. As a measure of a model's suitability, we may define

$$\epsilon^2(\mathbf{m}) = \frac{1}{K} \sum_{i=1}^{K} \left(\frac{D_i(\mathbf{m}) - D_i^0}{D_i^0}\right)^2. \tag{105}$$

Equations 104 constitute a $K \times 3N$ set of linear equations in the components of $\delta\mathbf{m}$. We may not, in general, expect to find a unique $\delta\mathbf{m}$ exactly satisfying equations 104 for all possible cases.

Various methods of solution have been applied to the system 104 (Backus & Gilbert, 1967), (Anderson & Smith, 1968), (Smith & Franklin, 1969), (Jordan & Franklin, 1971). We adopt here a general technique proposed by Franklin (Franklin, 1969).

We rewrite equations 104 more compactly as

$$\mathbb{A}(\mathbf{m}^0) \cdot \delta\mathbf{m} = \mathbf{\Delta}(\mathbf{m}^0) \tag{106}$$

where $\mathbb{A}(\mathbf{m}^0)$ is the matrix whose elements a_{ij} are

$$a_{ij}(\mathbf{m}) = \left[\frac{\partial D_i}{\partial m_i}\right]_{\mathbf{m}} \tag{107}$$

and $\mathbf{\Delta}(\mathbf{m}^0)$ is the vector of data residuals whose i^{th} component is $D_i^0 - D_i(\mathbf{m}^0)$. We now regard equation 106 as a linear relation between three stochastic processes: a signal process, a data process and a noise process. $\delta\mathbf{m}$ is a sample of the signal process, and $\mathbf{\Delta}(\mathbf{m}^0)$ is the sum of a sample of the data process plus a sample of the noise process. Each process is taken to have zero expectation.

The use of stochastic techniques to solve equation 106 is based, in part, upon contemplation of some of the potential sources of error entering into the relation. The measured spectral values D_i^0 are contaminated by measurement error and possible mode misidentification. The physical system upon which measurements are made may deviate from the class of models $\mathfrak{M}$ in which $\mathbf{m}$ must lie. It is possible that there is no model $\mathbf{m}$ in $\mathfrak{M}$ that would then satisfy equation 101.

Let $\mathbf{R}^m$ denote the autocorrelation associated with the signal process $\delta\mathbf{m}$, and $\mathbf{R}^0$ denote the autocorrelation operator associated with the noise process. $\mathbf{R}^m$ is a $3N \times 3N$ square matrix whose $(i,j)^{\text{th}}$ component is the expectation of the product $\delta m_i \delta m_j$. $\mathbf{R}^0$ is defined analogously. The best linear estimate for $\delta\mathbf{m}$ is given by (Franklin, 1969):

$$\delta\mathbf{m} = \mathbf{R}^m \cdot \mathbb{A}^T(\mathbf{m}^0) \cdot \left[\mathbb{A}(\mathbf{m}^0) \cdot \mathbf{R}^m \cdot \mathbb{A}^T(\mathbf{m}^0) + \mathbf{R}^0\right]^{-1} \cdot \mathbf{\Delta}(\mathbf{m}^0). \tag{108}$$

A solution, $\delta\mathbf{m}$, can be guaranteed to exist if $\mathbf{R}^0$ is a positive definite matrix.

The above method for computing $\delta\mathbf{m}$ was chosen, in preference to such techniques as least-squares solutions, because experience has indicated that the solution 108 is typically smaller and more stable than that provided by better known methods. Since equation 108 is used only to compute the perturbation $\delta\mathbf{m}$, which we use to iteratively improve $\mathbf{m}^0$, it does not follow that the errors in our "final" fit will correspond to any of the components of $\mathbf{R}^0$ or that the "distance" between our initial and final models will be strongly related to $\mathbf{R}^m$.

In practice, we take $\mathbf{R}^0$ to be a $K \times K$ diagonal matrix whose i^{th} diagonal element is the square of our estimate of the uncertainty of the i^{th} datum. $\mathbf{R}^m$ is also taken to be a diagonal matrix whose i^{th} element is taken equal to $\epsilon^2 q_i^2$, where ϵ is a small number (we used 0.2 to 0.01), and q_i is the i^{th} component of $\mathbf{m}$. Thus, we "suggest" to equation 108 that changes in a given component of $\mathbf{m}$ should be of the order of a fraction of its value. (Life is not quite that simple since, as Franklin (Franklin, 1969) points out, it is only the *ratio* of signal to noise that counts, but the values given above tend to work well in practice.)

It is also helpful to have some measure of the uncertainty associated with results so obtained. Such estimates must rely, of course, on the statistical properties we assign to errors in the data and errors in the model and the fashion in which one relates to the other. Forgoing this, we adopt here an estimate which is simple, and perhaps crude, in the extreme.

We define the r.m.s. absolute error in eigenfrequency ϵ_f as

$$\epsilon_f^2 = \frac{1}{K} \sum_{i=1}^{K} \Delta_i^2(\mathbf{m}). \tag{109}$$

Associated with each component m_i of $\mathbf{m}$ is an r.m.s. sensitivity σ_i defined by

$$\sigma_i^2 = \frac{1}{K} \sum_{j=1}^{K} a_{ji}^2(\mathbf{m}). \tag{110}$$

We take ϵ_f/σ_i as a measure of the uncertainty in m_i. If the data depend only weakly upon m_i, then σ_i will be small and ϵ_f/σ_i large. Similarly, if the data depend strongly on m_i, ϵ_f/σ_i will be (relatively) large. This error estimate assumes that all of the error of fit arises from a single parameter, and is clearly a worst case.

9 Experimental and Numerical Results

9.1 Illustrative applications

In order to render more specific the developments of preceding sections, we give, first, the results of two experiments and various aspects of their interpretation. The first sample discussed here was a 4-in.-diam. sphere of Lucite, formed by machining from a section of bar stock.

Figure 1 shows the observed forced spectrum of this sample as recorded by a swept-frequency analyzer. The sample was moderately clamped between a quartz transducer and a PZT–4 transducer, which happened to be available, and was in a refrigerated cabinet at about $-40°$C. The numbers are peak frequencies in kilohertz, as measured with a counter, and the mode assignments were made on the basis of considerations outlined below.

From past experience, it was possible to readily identify the "main sequence" of modes ${}_0S_2, {}_0S_3, \ldots$ all of which have substantial maxima and which, for l in excess of 2, tend to be more or less evenly spaced. Since, as we shall show, the properties of this sequence are generally dominated by shear velocity over regions of Poisson's ratio of common interest, it was desirable to identify at least one of ${}_0S_0$ or ${}_0S_1$, both of which are significantly influenced by compressional velocity. In identifying ${}_0S_0$, we applied two useful guides, gleaned from contemplation of equation 91:

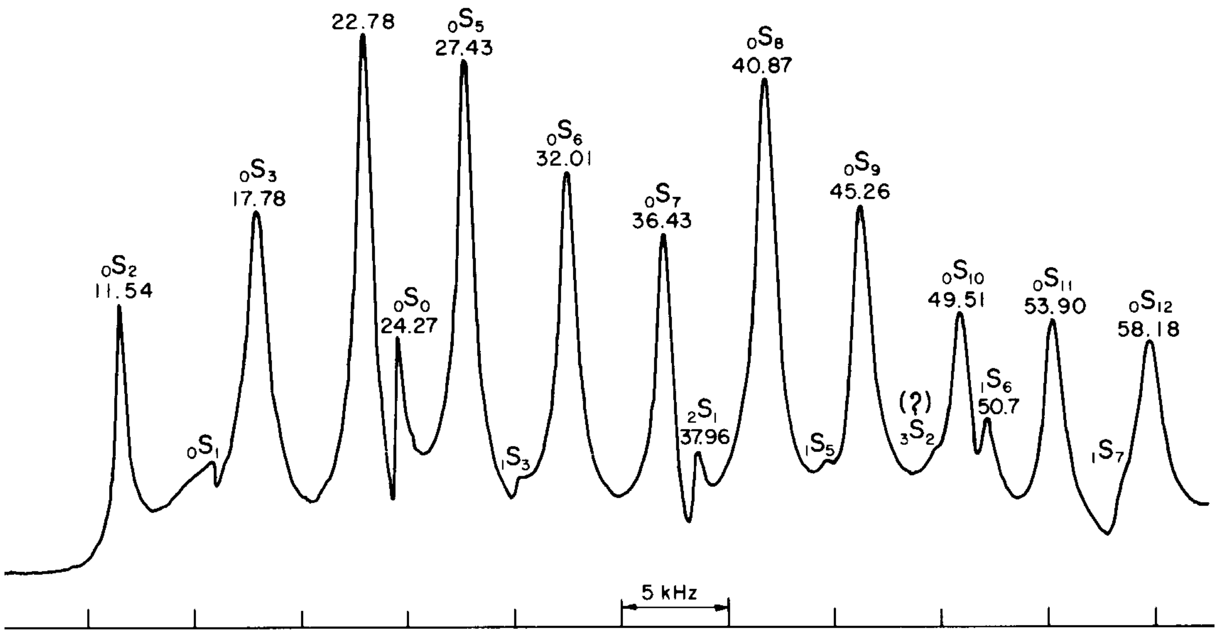

Figure 1: Observed forced response spectrum of a 4-in.-diam. Lucite sphere at −40°C. Ordinate is linear and arbitrary. Mode assignments and peak frequencies are show in kilohertz.

1. Adjacent modes both having l even or l odd will interfere destructively.

2. Adjacent modes not both having the same parity will interfere constructively.

These guides apply to frequencies lying between the two appropriate eigenfrequencies. In light of these, we interpret the sharp asymmetry of ${}_0S_0$ as being a result of destructive interference with ${}_0S_4$ on the left.

From these data, we estimated that V_p was about 2.84 km/sec and V_s was about 1.44 km/sec. Using these values we carried out forward calculations for all spheroidal modes having frequencies less than 10^5 Hz, the results of which are shown in Figures 2 and 3.

Figure 2 depicts the source factors, ${}_nA_l$, for the fundamental and first four overtones. These results confirm the identity of the main sequence and ${}_0S_0$, and permit the identification of a number of additional modes. Most of these are fairly deeply buried in the "noise" and are useless as data but they do help confirm our identifications. Prior to the use of these source factors, and the interference rules, we often found that our results were marred by uncertainty about mode identification. The above aids have greatly improved this aspect of the technique.

Figure 3 shows the quantity

$$\frac{\widetilde{Q}_\beta}{(\widetilde{Q}_\alpha + \widetilde{Q}_\beta)}$$

where $\widetilde{Q}_\alpha$ and $\widetilde{Q}_\beta$ are the weights computed from equation 77 to average the inverse Q's of compressional and shear waves to arrive at a mode's lumped inverse Q. (Actually, $\widetilde{Q}_\alpha + \widetilde{Q}_\beta = 1$, but the above form is more indicative.) In addition to being inherently significant, this quantity is a convenient, normalized index of the partition of energy into

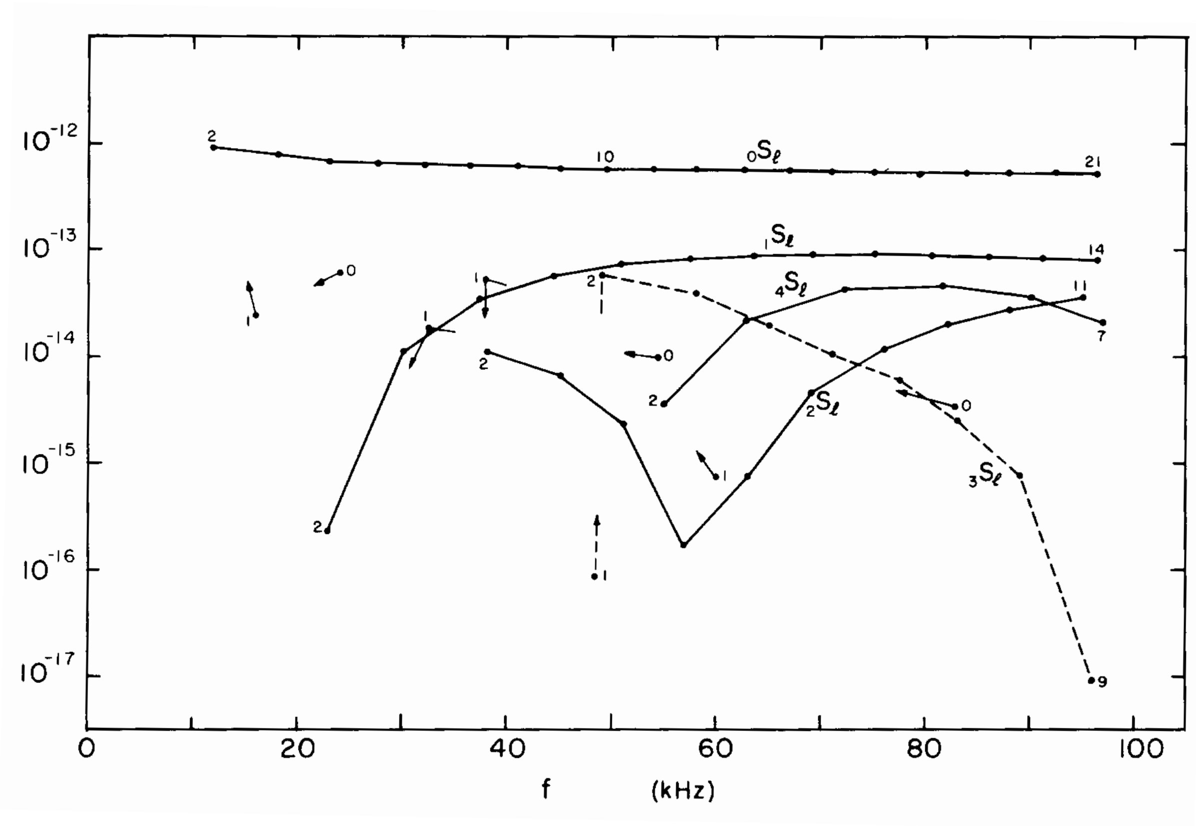

Figure 2: Source factors, $_nA_l$, for spheroidal modes of a 4-in.-diam. Lucite sphere at -40°C. Ordinate is logarithmic. Arrows for $l = 0$ and $l = 1$ indicate the overtone assignments for the lowest modes in each overtone series.

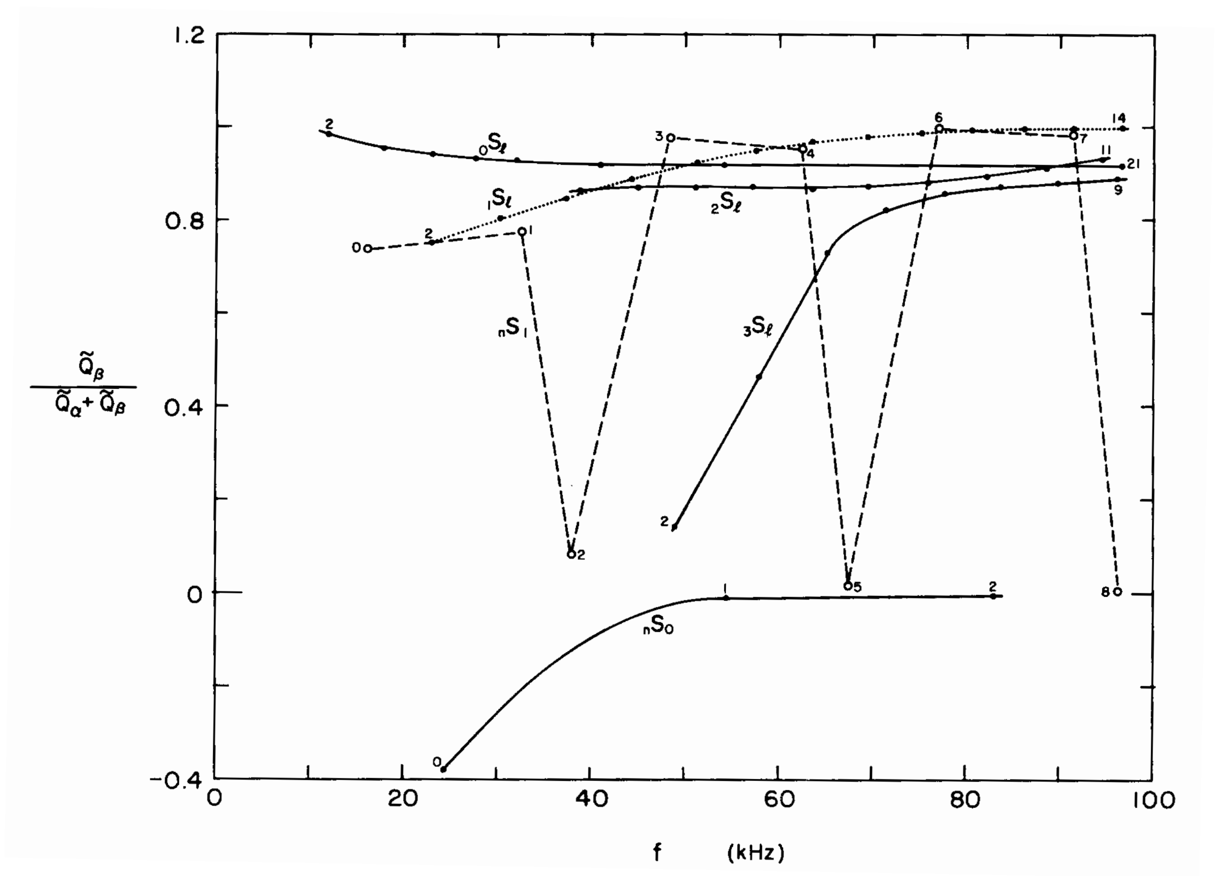

Figure 3: Relative attenuation partition coefficients for a 4-in.-diam. Lucite sphere at −40°C.

compressional and shear waves and thus of the properties "controlling" a given mode. (The two families ${}_nS_0$ and ${}_nS_1$ have been joined by separate curves.) Figure 3 suggests that the main sequence is dominated by shear velocity and almost uniformly so. We should not expect, then, to get good values for compressional velocity from this set alone. The set ${}_nS_l$ for $n = 2, 5, 8,$ *etc.* is controlled by V_p but does not usually show up well on observed spectra. Experience indicates that ${}_0S_0$, and to a lesser extent ${}_0S_1$, provide the most commonly observed control on V_p. Other modes are useful only when Q is sufficiently high that they appear clearly.

In this instance, as Figure 1 shows, Q is so low that we cannot set a baseline in order to estimate peak widths. For higher Q materials, we are sometimes able to measure main sequence attenuations from peak widths. We are seldom able to get reliable Q's for ${}_0S_0$ or other compression-dominated modes. Similar difficulties were reported by Fraser (Fraser, 1970) in vitreous silica, and it does not seem likely that we will be able to get reliable compressional attenuation data in any simple fashion.

This gloomy statement is bolstered by theoretical computations of the forced response using equation 91 and assumed values of Q_α and Q_β. Figure 4 shows the theoretical ${}_0S_4 - {}_0S_0$ interaction when Q_α and Q_β are both equal to 500. (These results are based on calculations for the 4-in. Lucite sphere.) In addition to the resemblance of Figure 4 to Figure 1, we note that ${}_0S_0$ still possesses substantial asymmetry even though the two peaks are (in this case) about 32 peak-widths apart.

Figure 5 depicts the interaction of ${}_1S_4$, ${}_2S_1$ and ${}_2S_2$ with ${}_0S_7$ on the left and ${}_0S_8$ on the right. Calculations for two values of $Q_\alpha = Q_\beta$ are shown. The asymmetry of each of ${}_1S_4$ and ${}_2S_1$ is clearly due to interaction with the more distant main sequence modes rather than with each other. The appearance of all three modes is dominated by their positions on the "tail" of ${}_0S_7$. The figure also depicts the rapid degradation of low

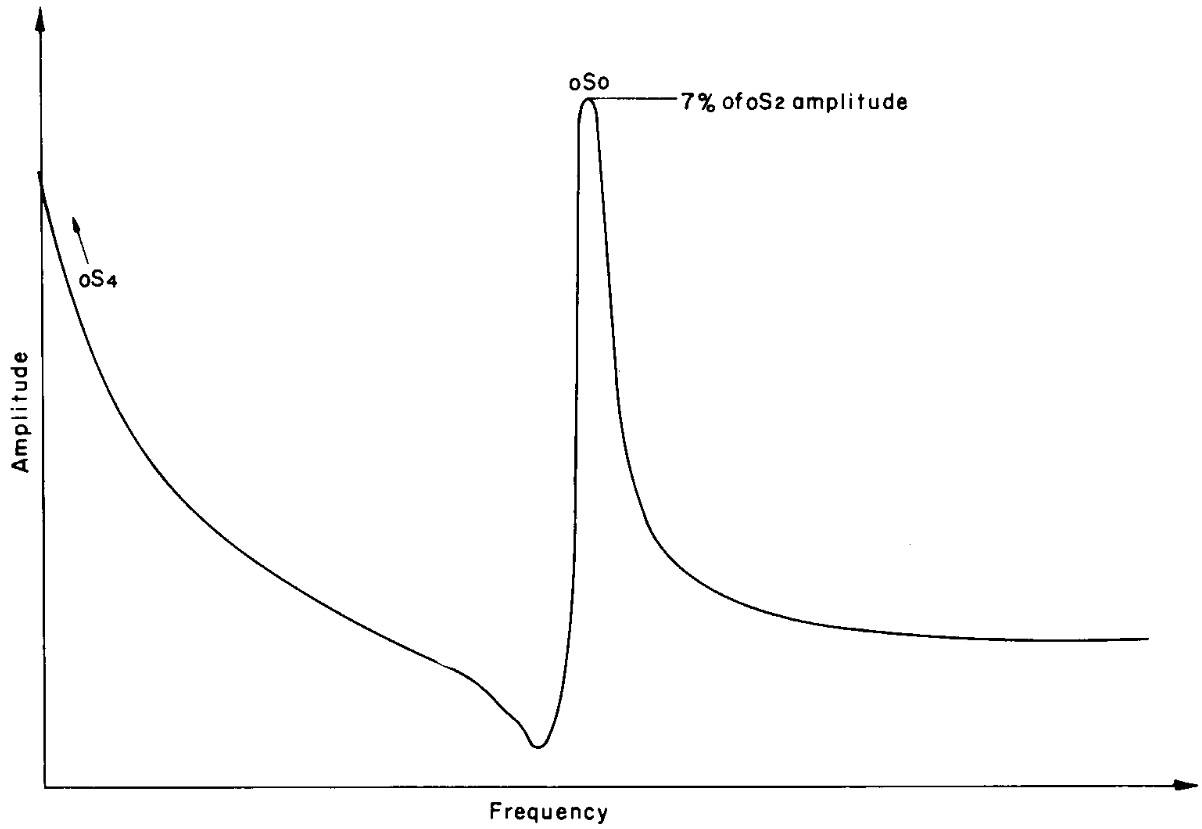

Figure 4: Portion of the theoretical forced response spectrum of a 4-in.-diam. Lucite sphere assuming $Q_\alpha = Q_\beta = 500$. The peak is ${}_0S_0$ and is asymmetric due to destructive interference on the left with ${}_0S_4$.

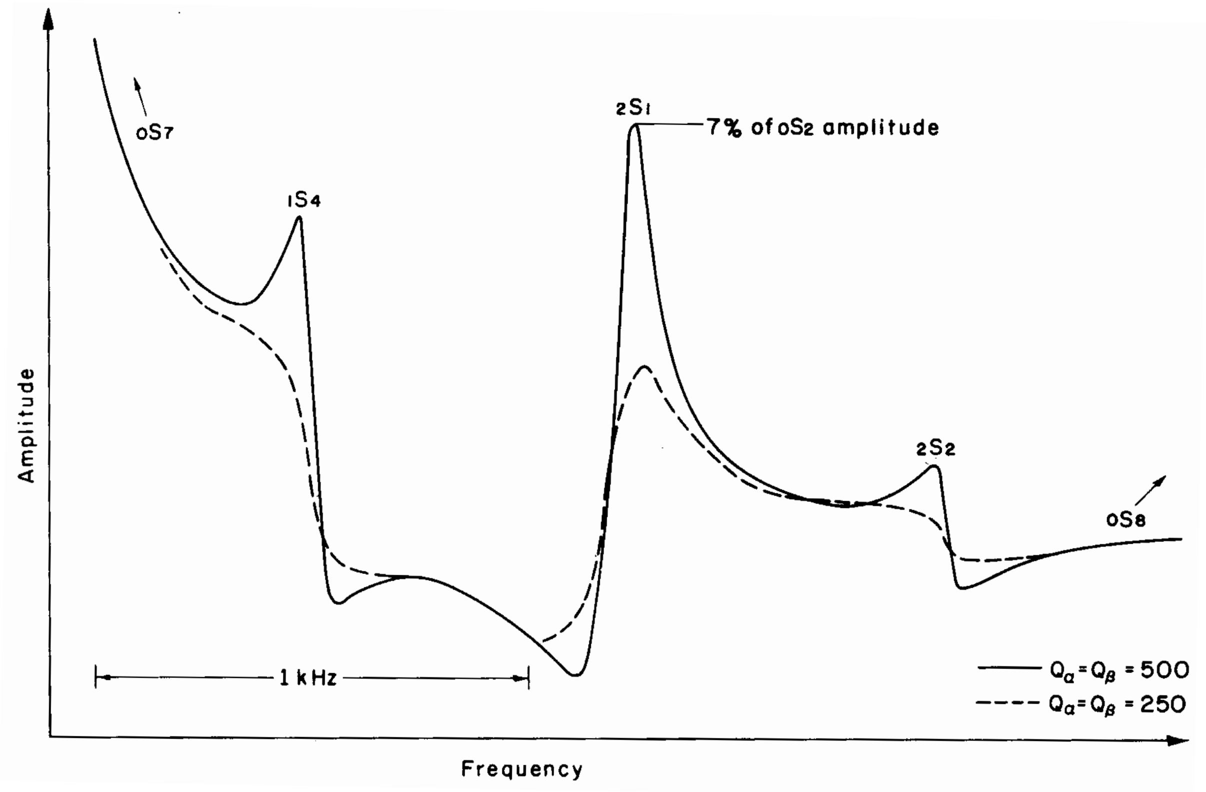

Figure 5: Portion of the theoretical forced response spectrum of a 4-in.-diam. Lucite sphere for two assumed values of $Q_\alpha = Q_\beta$. The figure depicts the effects of interference on ${}_0S_4$, ${}_2S_1$ and ${}_2S_2$.

amplitude modes with decreasing Q. The maxima associated with ${}_1S_4$ and ${}_2S_2$ become increasingly blurred as Q decreases. In the case of Lucite, which has a compressional Q of about 70, Figure 1 shows that only ${}_2S_1$ persists as a noticeable maximum.

We attempted, next, to "invert" the data obtained from the main sequence, plus ${}_0S_0$, in three different ways. The results of this endeavor are given in Table I.

The first result, Inverse A, was obtained by using all the data in the automated algorithm. The "fit" has an r.m.s. relative error of 1%, due largely to the 2.6% error in matching ${}_0S_2$. Inverse B was obtained by manually matching ${}_0S_0$ and ${}_0S_9$. This result has the same r.m.s. relative error despite an increase in the error for ${}_0S_2$, and further suggests that ${}_0S_2$ is behaving anomalously. The third result, Inverse C, was obtained by using all the data *except* ${}_0S_2$, and still has an r.m.s. relative error of 1%. The constancy of this number is, so far as we know, fortuitous. However, if we omit ${}_0S_2$ entirely, the error drops to 0.09%. It is not, in our experience, unusual for the mode ${}_0S_2$ to be inconsistent with remaining modes. We cannot offer an explanation of this observation at this time but do recommend that, when sufficient alternative data are available, it not be utilized. We may observe, however, that of the suite of surface wave modes, ${}_0S_2$, ${}_0S_3$, *etc.*, ${}_0S_2$ does possess the smallest surface wave number, $(l + \frac{1}{2})/a$.

Table II shows the result of an inversion of data from a 4-in. GE–125 fused quartz sphere at 19°C. The error is 0.03% and ${}_0S_2$ does not show anomalous behavior. These results are unusually good. We note that the relative errors suggest that computed frequencies for the main sequence are deviating systematically from observed frequencies. Since modes of the form ${}_0S_l$ are known, for increasing l, to become increasingly concentrated near the surface, we may speculate that such systematic errors imply a lower-velocity surficial region. Other candidates are geometrical irregularities, influence of the transducers, *etc.* We introduce this point because Fraser (Fraser, 1970) has shown that vacuum

Table I: Comparison of velocity estimates.

Mode	Observed	Inverse A		Inverse B		Inverse C	
	kHz	kHz	$\frac{\text{Obs}-\text{Comp}}{\text{Obs}}$	kHz	$\frac{\text{Obs}-\text{Comp}}{\text{Obs}}$	kHz	$\frac{\text{Obs}-\text{Comp}}{\text{Obs}}$
${}_0S_0$	24.27	24.41	-5.8×10^{-3}	24.29	-8.2×10^{-4}	24.27	1.28×10^{-4}
${}_0S_2$	11.54	11.84	-2.6×10^{-2}	11.92	-3.3×10^{-2}	11.91	-3.2×10^{-2}
${}_0S_3$	17.78	17.64	7.9×10^{-3}	17.77	5.6×10^{-4}	17.75	1.65×10^{-3}
${}_0S_4$	22.78	22.63	6.6×10^{-3}	22.79	-4.3×10^{-4}	22.78	3.99×10^{-4}
${}_0S_5$	27.43	27.30	4.7×10^{-3}	27.50	-2.5×10^{-3}	27.47	-1.44×10^{-3}
${}_0S_6$	32.01	31.82	5.9×10^{-3}	32.04	-9.4×10^{-4}	32.01	-6.0×10^{-6}
${}_0S_7$	36.43	36.25	4.9×10^{-3}	36.50	-1.9×10^{-3}	36.46	-8.7×10^{-4}
${}_0S_8$	40.87	40.62	6.1×10^{-3}	40.90	-7.3×10^{-4}	40.86	3.2×10^{-4}
${}_0S_9$	45.26	44.95	6.8×10^{-3}	45.26	0	45.21	1.0×10^{-3}
${}_0S_{10}$	49.51	49.26	5.0×10^{-3}	49.60	-1.8×10^{-3}	49.54	-6.9×10^{-4}
rms error			1.0×10^{-2}		1.0×10^{-2}		1.0×10^{-2}

Observed 5.08-cm-radius Lucite sphere at -40°C

Inverse A Computed using all data shown

$V_p = 284262$

$V_s = 142577$

Inverse B Estimated for fit to ${}_0S_0$ and ${}_0S_9$

$V_p = 283864$

$V_s = 143650$

Inverse C Computed using all but ${}_0S_2$

$V_p = 283566$

$V_s = 143504$

Table II: Inversion of data from a 4-in.-diameter sample of GE–125 fused quartz at 19°C.

Mode	Observed (Hz)	Computed (Hz)	$\frac{(\text{Obs} - \text{Comp})}{\text{Obs}}$
$_0S_2$	30898.0	30894.2	1.23×10^{-4}
$_0S_1$	38016.7	38045.7	-7.64×10^{-4}
$_0S_0$	44555.0	44545.8	2.07×10^{-4}
$_0S_3$	45579.7	45569.4	2.27×10^{-4}
$_0S_4$	58088.3	58084.5	6.65×10^{-5}
$_0S_5$	69825.9	69821.5	6.27×10^{-5}
$_0S_6$	81202.6	81201.6	1.28×10^{-5}
$_0S_7$	92382.6	92387.1	-4.86×10^{-5}

R.M.S. Relative error	3.0×10^{-4}
Computed velocities	$V_p = 593681$ cm/sec
	$V_s = 375303$ cm/sec

heating of some vitreous silicas strongly influences the attenuation of various torsional (shear) modes.

Interferometric techniques such as this are particularly useful for gauging the influence of variables such as temperature on velocities. It is often possible to "track" variations in velocities which are smaller than the errors of measurement. Each additional set of data is easily interpreted as a perturbation of the previous set and does not require additional mode identification. Figure 6 shows results obtained from Lucite and fused quartz at three different temperatures. The data are shown as variations relative to values measured at 21°C. We have estimated temperature variations in the cabinet at

$\pm 1°C$ and these are depicted as horizontal error bars. The linearity of the temperature dependence of elastic velocities in Lucite is striking. The slight negative temperature dependence of fused quartz is consistent with results described by Mason (Mason, 1958). (These data are shown purely for purposes of demonstration.)

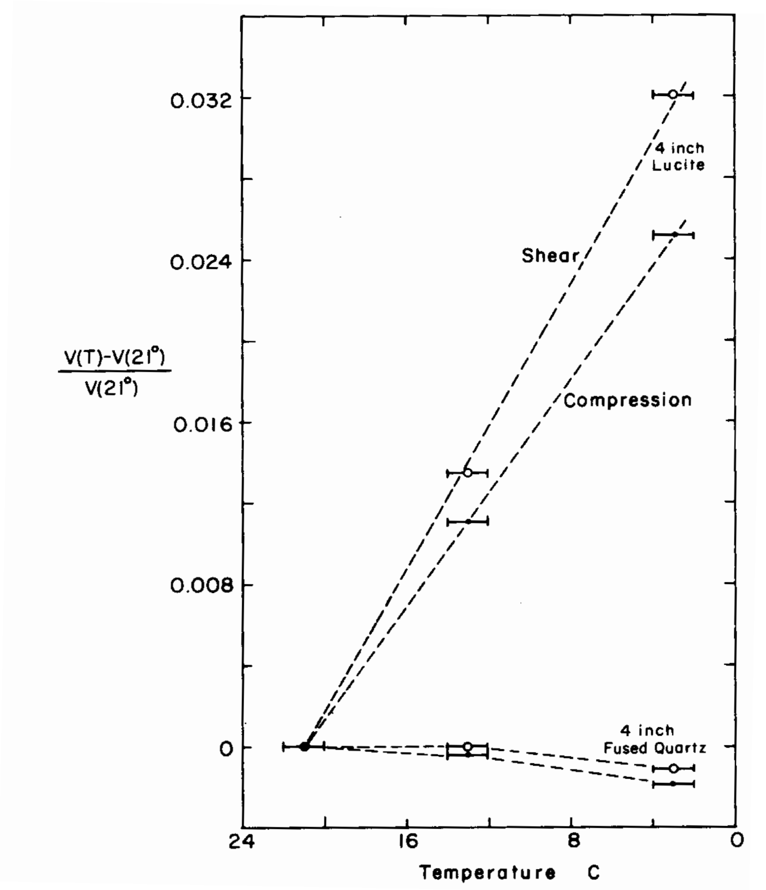

Figure 6: Inferred relative variations of compressional and shear velocities in 4-in.-diam. spheres of Lucite and GE–125 fused quartz, with temperature. Results are shown as a relative change, for each quantity, from its value at 21°C.

9.2 Some general results and a graphical inversion method

Figure E1 (Appendix E) depicts the variation of the dimensionless frequency of various spheroidal modes of a homogeneous sphere as a function of the ration of shear and compressional velocities. The dimensionless frequency ${}_nf_l^*$ is related to the actual frequency ${}_nf_l$ (we have used Hertz here) by

$$ {}_nf_l^* = \left(\frac{r_N}{V_p}\right) {}_nf_l. $$

In addition, Poisson's ratio is shown for those values of V_s/V_p for which it is positive.

The loci of all modes shown, except ${}_0S_0$, appear to converge on the origin as linear homogeneous functions of V_s/V_p. ${}_0S_2$ remains substantially linear for V_s/V_p as great as 0.625. Clearly modes which behave in this fashion are virtually independent of compressional velocity and Figure E1 confirms our earlier statements about the sensitivity of various modes to compressional and shear velocities. The left-hand side of the figure would have been more manageable if V_s had been used to nondimensionalize frequency instead of V_p. We took the point of view, however, that in experimental work one is more likely, if any prior data are available, to have an estimate for V_p.

On the other extreme, calculations were carried to the "Limit of Elastic Stability," indicated in the figure. This limit is imposed by the condition of a non-negative compressibility and corresponds to a Poisson's ration of -1. So far as we are aware, any requirement of a non-negative Poisson's ratio is based strictly on intuitive and empirical grounds.

Figure E2 is a plot of the ratio of frequency for several pairs of modes (dimensionless or otherwise) as a function of V_s/V_p. The ratios ${}_0f_0/{}_0f_2$, ${}_0f_0/{}_0f_3$, and ${}_0f_1/{}_0f_2$ are shown using the scale on the left, and ${}_0f_3/{}_0f_2$ is shown using the greatly expanded scale on the right. Figure E2 implies that the pair ${}_0f_2$ and ${}_0f_3$ will not serve well to determine V_s/V_p, whereas ${}_0f_0$ and ${}_0f_3$ or ${}_0f_2$ will. The pair ${}_0f_1$ and ${}_0f_2$ is of questionable value.

The plots are useful as a means of graphical inversion, as we shall now show from the data of Table III. For the 4-in. fused quartz specimen we have

$$\frac{{}_0f_0}{{}_0f_2} = \frac{44555}{30898} = 1.4420$$
$$\frac{{}_0f_0}{{}_0f_3} = \frac{44555}{45580} = 0.9775$$

and

$$\frac{{}_0f_3}{{}_0f_2} = \frac{45580}{30898} = 1.47517$$

which imply (from Figure E2)

$$\frac{V_s}{V_p} = 0.631,\ 0.633 \text{ and } 0.631.$$

For $V_s/V_p = 0.632$, Figure E1 gives

$$\frac{{}_0f_0\, r_N}{V_p} = 0.3807$$

or

$$V_p = 594535$$

and

$$V_s = 375746$$

which differ about 0.2% from the values determined by automated inversion.

This method should provide usefully accurate results when individual data are of a fairly high quality — as is often the case for isotropic, high-Q materials. When only data of lower quality are available, or greater precision would be useful, we must use some sort of automated algorithm.

Table III:

$$\text{Forward computation for } V_p = 593980 \text{ cm/sec}$$
$$V_s = 375540 \text{ cm/sec}$$

$${}_0f_0 = 44563.05$$
$${}_0f_2 = 30913.44$$
$${}_0f_4 = 58119.63$$

Inverse computation

	Model 1			Model 2		
Pass no.	V_p	V_s	rms error	V_p	V_s	rms error
1	712766	450648	2×10^{-1}	475184	300432	2×10^{-1}
2	593768	375402	3.6×10^{-4}	594192	375678	3.6×10^{-4}
3	593980	375540	7.2×10^{-7}	593980	375540	6.4×10^{-7}

9.3 Automated inversion

The inversion of spectral data to yield elastic velocities is, even in our relatively simple case, a fundamentally nonlinear process. Consequently it is impossible to provide the proofs of uniqueness commonly available for linear problems. The more general problem of uniqueness when elastic properties are functions of radius has been extensively discussed (see, for example, (Backus & Gilbert, 1967)) but the results are not of much use to us here.

The monotonic dependence of the ratio of ${}_0f_0$ to ${}_0f_2$, and of the dimensionless frequency ${}_0f_0^*$, on V_s/V_p suggests that, within the range of V_s/V_p shown in Figure E2, inversion is unique if the proper data are used.

In a realistic application, however, we must account for several additional factors. The following effects may be important:

1. Measurement errors or contamination of the data by asphericity, anisotropy, inhomogeneity, a finite Q , and external influences.

2. Mode misidentification.

3. Numerical instability in the computing processes.

The result of either 1 or 2 may be to produce a set of data which *no* homogeneous sphere will fit. The influence of such errors will be heightened if we attempt to use contaminated data to determine a parameter which is only a slowly varying function of these data. Such a problem is said to be ill-posed and the effects of small errors in "ill-posed" computations are often quite large (see, as an example, (Franklin, 1968)).

While we have not devoted extensive attention to this problem, we have performed a few exploratory calculations. Table III shows the result of two inversions using artificial data. The starting models were chosen to be about 20% "away" from the known correct model. The process is rapidly convergent. We have also performed similar calculations with data to which a 1% random error was added. Such inversions no longer gave the correct answer but, in the few cases we tried, the answer remained independent of the starting model.

It is easy to conceive of various Monte Carlo experiments, requiring the usual spectacular amounts of computing time, which would help delimit, for a given data set, the error level at which inversion becomes "incoherent." Because of the large multiplicity of parameters required to cover just typical experimental cases, we do not presently think it worthwhile to do this. As a matter of experience, we have never, so far as we can tell, encountered any pathological results.

9.4 Errors

We will briefly discuss only one potential source of error: the effect of mechanical loading by transducers or support devices. Appendix D describes a computation which purports to estimate the perturbation in eigenfrequency induced by clamping, with a given force, a sphere against a halfspace of known elastic properties.

The errors so deduced do not exceed a few parts in 10^4 for a fairly realistic range of properties. We believe these results lend support to claims by Fraser and LeCraw (Fraser & LeCraw, 1964) and Francis Birch (personal communication) that this method is relatively free from errors arising from such sources.

References

Abramowitz, & Stegun. 1968.

Anderson, D. L. 1966. Recent evidence concerning the structure and composition of the earth's mantle. *In: Physics and Chemistry of the Earth*, vol. 6. Oxford: Pergamon Press.

Anderson, D. L., & Smith, M. L. 1968. *Mathematical and physical inversion of gross earth data*. Paper presented at Am. Geophys. Union Annual Meeting, Washington, D.C.

Anderson, O. L., & Soga, N. 1966. *Elastic constants of small sintered ceramic specimens*. Summary Technical Report AFML-TR-65-202. Air Force Materials Laboratory.

Anderson, O. L., Scholz, C., Soga, N., Warren, N., & Schrieber, E. 1970. Elastic properties of a microbreccia, igneous rock and lunar fines from Apollo 11 mission. *Pages 1959–1973 of: Proceedings of Apollo 11 Lunar Science Conference*, vol. 3.

Backus, G. E. 1967. Converting vector and tensor equations to scalar equations in spherical coordinates. *Geophysical J. of the Royal Astr. Soc.*, **13**, 71–101.

Backus, G. E., & Gilbert, J. F. 1967. Numerical applications of a formation for geophysical inverse problems. *Geophysical J. of the Royal Astr. Soc.*, **13**, 247–276.

Ben-Menahem, A. 1964. Mode-ray duality. *Bull. of the Seis. Soc. of America*, **54**, 1315–1321.

Coquin, G. A. 1964a. Attenuation of guided waves in isotropic viscoelastic materials. *J. Acous. Soc. of America*, **36**, 1074–1080.

Coquin, G. A. 1964b. *Free vibrations of viscoelastic spheres*. Paper presented at Acoust. Soc. of America Meeting, N.Y. City.

Dahlen, F. A. 1968. The normal modes of a rotating elliptical earth. *Geophysical J. of the Royal Astr. Soc.*, **16**, 329–367.

Franklin. 1969. manuscript.

Franklin, J. N. 1968. *Matrix theory.* New Jersey: Prentice Hall.

Fraser, D. B. 1968. Factors influencing the acoustic properties of vitreous silica. *J. Appl. Physics*, **39**, 5868–5878.

Fraser, D. B. 1970. Acoustic loss of vitreous silica at elevated temperatures. *J. Appl. Physics*, **41**, 6–11.

Fraser, D. B., & LeCraw, R. C. 1964. Novel method of measuring elastic and anelastic properties of solids. *Rev. Sci. Inst.*, **35**, 1113–1115.

Fung, Y. C. 1965. *Foundations of solid mechanics.* New Jersey: Prentice Hall.

Gilbert, J. F., & Backus, G. E. 1966. Propagator matrices in elastic wave and vibration problems. *Geophysics*, **31**, 326–332.

Harkrider, D. G. 1964. Surface waves in multilayered elastic media I. Rayleigh and Love waves from buried sources in a multilayered elastic half-space. *Bull. of the Seis. Soc. of America*, **54**, 627–679.

Hildebrand, F. B. 1956. *Introduction to numerical analysis.* New York: McGraw-Hill.

Hill, E. L. 1954. The theory of vector spherical harmonics. *American Journal of Physics*, **22**, 211–214.

Jordan, & Franklin. 1971. manuscript.

Mason. 1958.

Rayleigh, Lord. 1945. *Theory of sound.* New York: Dover.

Smith, M. L., & Franklin, J. N. 1969. Geophysical applications of generalized inverse theory. *Journal of Geophysical Research*, **74**, 2783–2785.

Soga, N., & Anderson, O. L. 1967. Elastic properties of tektites measured by resonant sphere technique. *Journal of Geophysical Research*, **72**, 1733–1739.

Sternberg, E. 1960. On the integration of the equations of motion in the classical theory of elasticity. *Arch. for Rat. Mech. and Anal.*, **6**, 34–50.

Timoshenko, S., & Goodier, J. N. 1951. *Theory of elasticity.* New York: McGraw-Hill.

A Analytic Solutions of the Transformed Wave Equation

We represent $\mathbf{u}$ by

$$\mathbf{u} = \boldsymbol{\nabla}\psi + \boldsymbol{\nabla} \times \widehat{\mathbf{r}} r\chi + \boldsymbol{\nabla} \times \boldsymbol{\nabla} \times \widehat{\mathbf{r}} r\sigma \tag{A1}$$

where ψ, χ and σ are scalar fields. The representation A1 was chosen because it is "natural" to the field equations (equation 3).

It is helpful to develop the following the useful expressions

$$\boldsymbol{\nabla} \cdot \mathbf{u} = \nabla^2 \psi,$$

and

$$\begin{aligned}
\boldsymbol{\nabla} \times \boldsymbol{\nabla} \times \mathbf{u} &= \boldsymbol{\nabla} \times \boldsymbol{\nabla} \times \boldsymbol{\nabla} \times (\widehat{\mathbf{r}} r\chi) + \boldsymbol{\nabla} \times \boldsymbol{\nabla} \times \boldsymbol{\nabla} \times \boldsymbol{\nabla} \times (\widehat{\mathbf{r}} r\sigma) \\
&= \boldsymbol{\nabla} \times \left\{ \boldsymbol{\nabla} \left(\boldsymbol{\nabla} \cdot \widehat{\mathbf{r}} r\chi \right) - \nabla^2 \left(\widehat{\mathbf{r}} r\chi \right) \right\} \\
&+ \boldsymbol{\nabla} \times \boldsymbol{\nabla} \times \left\{ \boldsymbol{\nabla} \left(\boldsymbol{\nabla} \cdot \widehat{\mathbf{r}} r\sigma \right) - \nabla^2 \left(\widehat{\mathbf{r}} r\sigma \right) \right\}.
\end{aligned}$$

We expand $\nabla^2 (\widehat{\mathbf{r}} r\chi)$ as

$$\begin{aligned}
\nabla^2 (\widehat{\mathbf{r}} r\chi) &= \widehat{\mathbf{r}} \left\{ \nabla^2 (r\chi) - \frac{2}{r}\chi \right\} + \boldsymbol{\nabla}_1 \left\{ \frac{2}{r}\chi \right\} \\
&= \widehat{\mathbf{r}} r \nabla^2 \chi + \boldsymbol{\nabla} \{2\chi\}
\end{aligned}$$

as may easily be shown by expanding. So,

$$\boldsymbol{\nabla} \times \boldsymbol{\nabla} \times \mathbf{u} = -\boldsymbol{\nabla} \times \widehat{\mathbf{r}} r \nabla^2 \chi - \boldsymbol{\nabla} \times \boldsymbol{\nabla} \times \widehat{\mathbf{r}} r \nabla^2 \sigma.$$

If we insert these into the field equation (equation 3) and regroup terms, we find

$$\begin{aligned}
\boldsymbol{\nabla} \left\{ \rho \partial_t^2 \psi - (\lambda + 2\mu) \nabla^2 \psi \right\} + \boldsymbol{\nabla} \times \widehat{\mathbf{r}} r \left\{ \rho \partial_t^2 \chi - \mu \nabla^2 \chi \right\} + & \\
\boldsymbol{\nabla} \times \boldsymbol{\nabla} \times \widehat{\mathbf{r}} r \left\{ \rho \partial_t^2 \sigma - \mu \nabla^2 \sigma \right\} &= 0.
\end{aligned}$$

In order to ensure that equation 3 is satisfied, it is sufficient that ψ, χ and σ be solutions to

$$\rho\partial_t^2\psi - (\lambda + 2\mu)\,\nabla^2\psi = 0, \tag{A2a}$$

$$\rho\partial_t^2\chi - \mu\nabla^2\chi = 0, \tag{A2b}$$

and

$$\rho\partial_t^2\sigma - \mu\nabla^2\sigma = 0. \tag{A2c}$$

We have not shown that all solutions to equation 3 can be expressed in terms of functions satisfying equations A2 and A1. These solutions are, however, known to be complete (Sternberg, 1960).

We now Fourier transform the system and introduce the expansions

$$\psi(r,\theta,\phi,\omega) = \sum_{l=0}^{\infty}\sum_{m=-l}^{l} \psi_l^m(r,\omega)\,Y_l^m(\theta,\phi), \tag{A3a}$$

$$\chi(r,\theta,\phi,\omega) = \sum_{l=1}^{\infty}\sum_{m=-l}^{l} \chi_l^m(r,\omega)\,Y_l^m(\theta,\phi), \tag{A3b}$$

and

$$\sigma(r,\theta,\phi,\omega) = \sum_{l=1}^{\infty}\sum_{m=-l}^{l} \sigma_l^m(r,\omega)\,Y_l^m(\theta,\phi). \tag{A3c}$$

The terms of degree $l = 0$ in the expansions for χ and σ have been omitted since they do not contribute to the displacement field.

The expansions A3a–A3c are inserted into the transformed versions of A2a–A2c. We make use of equation 6 and 14 to simplify the result. If f is some scalar field, then by equation 6

$$\boldsymbol{\nabla} f = \widehat{\mathbf{r}}\partial_r f + \boldsymbol{\nabla}_1\left(r^{-1} f\right)$$

and

$$\nabla^2 f = \partial_r^2 f + \frac{2}{r}\partial_r f + r^{-2}\nabla_1^2 f. \tag{A4}$$

The resulting expressions are multiplied by $Y_l^m(\theta,\phi)^\dagger \sin\theta$ and integrated over θ and ϕ. We appeal to the orthogonality relation 12. We then have

$$\left\{\partial_r^2 + \frac{2}{r}\partial_r + \frac{\omega^2\rho}{\lambda+2\mu} - \frac{l(l+1)}{r^2}\right\}\psi_l^m(r,\omega) = 0, \tag{A5a}$$

$$\left\{\partial_r^2 + \frac{2}{r}\partial_r + \frac{\omega^2\rho}{\mu} - \frac{l(l+1)}{r^2}\right\}\chi_l^m(r,\omega) = 0 \tag{A5b}$$

and

$$\left\{\partial_r^2 + \frac{2}{r}\partial_r + \frac{\omega^2\rho}{\mu} - \frac{l(l+1)}{r^2}\right\}\sigma_l^m(r,\omega) = 0. \tag{A5c}$$

Each of the operators in brackets is some form of the spherical Bessel's operator. Its solutions are well-known and they are

$$\psi_l^m = A_l^m(\omega) j_l(kr) + B_l^m(\omega) y_l(kr), \tag{A6a}$$

$$\chi_l^m = C_l^m(\omega) j_l(\gamma r) + D_l^m(\omega) y_l(\gamma r), \tag{A6b}$$

and

$$\sigma_l^m = E_l^m(\omega) j_l(\gamma r) + F_l^m(\omega) y_l(\gamma r), \tag{A6c}$$

where

$$k = \frac{\omega}{\sqrt{\dfrac{\lambda+2\mu}{\rho}}} \tag{A7}$$

and

$$\gamma = \frac{\omega}{\sqrt{\dfrac{\mu}{\rho}}}. \tag{A8}$$

We wish now to relate U, V and W to ψ, χ and σ. To do this, we will rearrange equation A1 to resemble equation 4. For convenience we will drop subscripts and superscripts.

We note immediately that

$$\boldsymbol{\nabla}\psi = \widehat{\mathbf{r}}\partial_r\psi + \boldsymbol{\nabla}_1\left(r^{-1}\psi\right).$$

Also,

$$\begin{aligned}\boldsymbol{\nabla}\times\widehat{\mathbf{r}}r\chi &= r\chi\boldsymbol{\nabla}\times\widehat{\mathbf{r}} - \widehat{\mathbf{r}}\times\boldsymbol{\nabla}(r\chi)\\ &= -\widehat{\mathbf{r}}\times\boldsymbol{\nabla}(r\chi)\\ &= -\widehat{\mathbf{r}}\times\boldsymbol{\nabla}_1\chi.\end{aligned}$$

The third term can be expanded as

$$\begin{aligned}\boldsymbol{\nabla}\times\boldsymbol{\nabla}\times\widehat{\mathbf{r}}r\sigma &= \boldsymbol{\nabla}\left(\boldsymbol{\nabla}\cdot\widehat{\mathbf{r}}r\sigma\right) - \nabla^2\left(\widehat{\mathbf{r}}r\sigma\right)\\ &= -\widehat{\mathbf{r}}r\nabla^2\sigma - \boldsymbol{\nabla}(2\sigma) + \boldsymbol{\nabla}\left[r^{-2}\partial r\left(r^3\sigma\right)\right]\\ &= \widehat{\mathbf{r}}\left\{-r\nabla^2\sigma + \partial_r\left[r^{-2}\partial_r\left(r^3\sigma\right) - 2\sigma\right]\right\} + \boldsymbol{\nabla}_1\left\{r^{-3}\partial_r\left(r^3\sigma\right) - 2r^{-1}\sigma\right\}\\ &= \widehat{\mathbf{r}}\left\{r^{-1}\nabla^2\sigma\right\} + \boldsymbol{\nabla}_1\left\{r^{-1}\sigma + \partial_r\sigma\right\}\\ &= \widehat{\mathbf{r}}\left\{\frac{-l(l+1)}{r}\sigma\right\} + \boldsymbol{\nabla}_1\left\{r^{-1}\partial_r(r\sigma)\right\}.\end{aligned}$$

Collecting these we have

$$\mathbf{u} = \widehat{\mathbf{r}}\left\{\partial_r\psi - \frac{l(l+1)}{r}\sigma\right\} + \boldsymbol{\nabla}_1\left\{r^{-1}\psi + r^{-1}\partial_r(r\sigma)\right\} - r\times\boldsymbol{\nabla}_1\chi.$$

Therefore

$$U_l^m = \partial_r\psi_l^m - \frac{l(l+1)}{r}\sigma_l^m, \tag{A9a}$$

$$V_l^m = r^{-1}\left[\psi_l^m + \partial_r\left(r\sigma_l^m\right)\right] \tag{A9b}$$

and

$$W_l^m = \chi_l^m. \tag{A9c}$$

B The Traction on a Spherical Surface

Let $\mathbb{T}$ be the elastic stress tensor resulting from a displacement field $\mathbf{u}$. $\mathbb{T}$ is given by

$$\mathbb{T} = \lambda(\boldsymbol{\nabla} \cdot \mathbf{u})\mathbb{I} + \mu(\boldsymbol{\nabla}\mathbf{u} + \mathbf{u}\boldsymbol{\nabla}) \tag{B1}$$

where $\mathbf{u}\boldsymbol{\nabla}$ is simply the transpose of $\boldsymbol{\nabla}\mathbf{u}$. The force (not stress) acting across a surface whose unit normal is $\vec{n}$ is given by $\vec{n} \cdot \mathbb{T}$, which is a vector quantity. We represent the force acting across a surface whose normal is the radius vector $\widehat{\mathbf{r}}$ by

$$\widehat{\mathbf{r}} \cdot \mathbb{T} = \widehat{\mathbf{r}}P + \boldsymbol{\nabla}_1 Q - \widehat{\mathbf{r}} \times \boldsymbol{\nabla}_1 R. \tag{B2}$$

Our problem is to relate the scalars P, Q and R to the scalars U, V and W which characterize the displacement field.

We note first that

$$\widehat{\mathbf{r}} \cdot \mathbb{T} = \lambda(\boldsymbol{\nabla} \cdot \mathbf{u})\widehat{\mathbf{r}} + \mu\widehat{\mathbf{r}} \cdot \{\boldsymbol{\nabla}\mathbf{u} + \mathbf{u}\boldsymbol{\nabla}\}. \tag{B3}$$

The divergence of $\mathbf{u}$ can be expanded as

$$\boldsymbol{\nabla} \cdot \mathbf{u} = \left(\widehat{\mathbf{r}}\partial_r + r^{-1}\boldsymbol{\nabla}_1\right) \cdot (\widehat{\mathbf{r}}U + \boldsymbol{\nabla}_1 V) \tag{B4}$$

since

$$\begin{aligned}
\boldsymbol{\nabla} \cdot (-\widehat{\mathbf{r}} \times \boldsymbol{\nabla}_1 W) &= -\widehat{\mathbf{r}} \cdot (\boldsymbol{\nabla} \times \boldsymbol{\nabla}_1 W) \\
&= -\widehat{\mathbf{r}} \cdot (\widehat{\mathbf{r}} \times \boldsymbol{\nabla}\partial_r W) \\
&= 0
\end{aligned}$$

because $\widehat{\mathbf{r}} \times \boldsymbol{\nabla}\partial_r W$ must be normal to $\widehat{\mathbf{r}}$. Equation B4 can be written as

$$\boldsymbol{\nabla} \cdot \mathbf{u} = \partial_r U + r^{-1}\nabla_1^2 V + \widehat{\mathbf{r}}\partial_r \cdot \boldsymbol{\nabla}_1 V + r^{-1}\boldsymbol{\nabla}_1 \cdot \widehat{\mathbf{r}} U. \tag{B5}$$

The third term vanishes since ∂_r commutes with $\boldsymbol{\nabla}_1$, and $\boldsymbol{\nabla}_1\partial_r V$ is normal to $\widehat{\mathbf{r}}$. The fourth term is equal to $(2/r)U$ as may be seen by replacing $r^{-1}\boldsymbol{\nabla}_1$ with $\boldsymbol{\nabla} - \widehat{\mathbf{r}}\partial_r$, an equivalent expression. We then have

$$\boldsymbol{\nabla} \cdot \mathbf{u} = \left(\partial_r + \frac{2}{r}\right) U + r^{-1}\nabla_1^2 V. \tag{B6}$$

The term $\widehat{\mathbf{r}} \cdot \{\boldsymbol{\nabla}\mathbf{u} + \mathbf{u}\boldsymbol{\nabla}\}$ in equation B3 is more difficult to deal with. In terms of the coordinate representation of $\mathbf{u}$, (*i.e.* u_r, u_θ, and u_ϕ),

$$\begin{aligned} \widehat{\mathbf{r}} \cdot \{\boldsymbol{\nabla}\mathbf{u} + \mathbf{u}\boldsymbol{\nabla}\} =& \widehat{\mathbf{r}}\left(2\partial_r u_r\right) \\ &+ \widehat{\theta}\left[\frac{1}{r}\partial_\theta u_r + r\partial_r\left(\frac{u_\theta}{r}\right)\right] \\ &+ \widehat{\phi}\left[\frac{1}{r\sin\theta}\partial_\phi u_r + r\partial_r\left(\frac{u_\phi}{r}\right)\right]. \end{aligned} \tag{B7}$$

By inspection of equation 5 which explicitly gives the coordinate components of $\boldsymbol{\nabla}_1$, we see that equation B7 may be rewritten as

$$\widehat{\mathbf{r}} \cdot \{\boldsymbol{\nabla}\mathbf{u} + \mathbf{u}\boldsymbol{\nabla}\} = \widehat{\mathbf{r}}\left(2\partial_r u_r\right) + \boldsymbol{\nabla}_1\left(\frac{u_r}{r}\right) + r\partial_r\left[\frac{1}{r}\left(\widehat{\theta}u_\theta + \widehat{\phi}u_\phi\right)\right].$$

We note that ∂_r commutes with $\widehat{\theta}$ and $\widehat{\phi}$. The expression in square brackets represents the non-radial portion of $\mathbf{u}$ and must therefore be identical with $\boldsymbol{\nabla}_1 v - \widehat{\mathbf{r}} \times \boldsymbol{\nabla}_1 w$. Since u_r is identical with U, we have

$$\widehat{\mathbf{r}} \cdot \{\boldsymbol{\nabla}\mathbf{u} + \mathbf{u}\boldsymbol{\nabla}\} = \widehat{\mathbf{r}}\left(2\partial_r v\right) + \frac{1}{r}\boldsymbol{\nabla}_1 u + r\partial_r\left\{\frac{1}{r}\boldsymbol{\nabla}_1 v - \frac{1}{r}\widehat{\mathbf{r}} \times \boldsymbol{\nabla}_1 w\right\}$$

or

$$\widehat{\mathbf{r}} \cdot \{\boldsymbol{\nabla}\mathbf{u} + \mathbf{u}\boldsymbol{\nabla}\} = \widehat{\mathbf{r}}\left(2\partial_r u\right) + \boldsymbol{\nabla}_1\left[\frac{u}{r} + r\partial_r\left(\frac{1}{r}v\right)\right] - \widehat{\mathbf{r}} \times \boldsymbol{\nabla}_1\left[r\partial_r\left(\frac{1}{r}w\right)\right].$$

Combining the above results, we have

$$P = (\lambda + 2\mu)\partial_r u + \frac{2\lambda}{r} u + \frac{\lambda}{r}\nabla_1^2 v, \tag{B8a}$$

$$Q = \mu \left\{ \frac{u}{r} + r\partial_r \left(\frac{v}{r} \right) \right\}, \tag{B8b}$$

and

$$R = \mu \left\{ r\partial_r \left(\frac{w}{r} \right) \right\}. \tag{B8c}$$

C Numerical Techniques

We outline, briefly, in this appendix the numerical techniques used in this study to a) generate the suite of normal modes for a layered elastic sphere and b) evaluate various integrals of interest associated with these modes.

For a given l and ω, the generation of solution functions proceeds exactly as outlined in Section 3. The matrix inversion required by equations 45 and 46 was not done explicitly. We chose instead to solve two sets of simultaneous linear equations. The Crout Reduction (Hildebrand, 1956) was found to be particularly convenient.

Bessel functions were generated by using Miller's well-known recurrence algorithm (Abramowitz & Stegun, 1968). One consequence of this technique is that the accurate evaluation of a spherical Bessel function for many values of its argument, as required, say, for integration, is a time-consuming process. For such applications it would perhaps be more efficient to numerically solve Bessel's equation, but computer memory limitations did not permit the additional coding this required.

In practice, the program was assigned a model and a value of l and proceeded to compute trail solutions for evenly spaced values of frequency. As the computation proceeded, indicator variables, as explained in Section 3, were monitored for a change of sign, which was taken to indicate a zero crossing. When this occurred, an estimate was made of the location of the zero crossing and the algorithm described below was invoked to iteratively improve the estimate. In general, two applications of the following procedure sufficed to locate the eigenfrequency to within one part in 10^6.

Gilbert and Backus (Backus & Gilbert, 1967) observed that Rayleigh's principle could be utilized to improve estimates of eigenfrequencies obtained by coarser methods. Suppose that for some frequency ω, near an eigenvalue, ω^*, we have computed a trial solution and find that the stress-free surface condition cannot be met. We may apply Rayleigh's principle, or perturbation theory, to the solution we *have* generated to estimate the change in ω the elimination of surface stress would produce. The first order estimate for this change is given by

$$\delta\omega = (8\pi\omega)^{-1} \frac{\left\{U_l\left(r_N\right) P_l\left(r_N\right) + l(l+1)V_l\left(r_N\right) Q_l\left(r_N\right)\right\}}{\int_0^{r_N} \rho r^2 \left\{U_l^2(r) + l(l+1)V_l^2(r)\right\}\, dr}. \tag{C1}$$

(We will not derive equation C1 here.) We then replace ω by $\omega + \delta\omega$ and repeat the process. We chose to terminate the iteration when $|\delta\omega/(\delta\omega + \omega)|$ fell below 10^{-6}.

The last point we wish to mention is the evaluation of integrals of the form

$$I = \int_0^u Z(\mathbf{u})\, dr \tag{C2}$$

where Z is some operator on the solution functions, $U(r)$, *etc.* In general, we may expect Z to vary appreciably over a length L of about

$$L = \frac{2\pi V_p}{\omega} \tag{C3}$$

where V_p is the local compressional velocity. L is simply the wavelength of a compressional wave of angular frequency ω. In computing I, the program was designed to utilize steps not exceeding ϵL_i; where ϵ is a small ($\sim 3 \times 10^{-2}$) number and L_i is the scale length appropriate to a given shell. This technique yielded a reliably constant accuracy over many wide variations of scale without extracting undue computing labor for small values of ω.

D An Estimate of Transducer and Support Influences on Measured Eigenfrequencies

Perturbation due to an anchored spring

We suppose that one end of a spring of spring constant k is affixed to a point P on the surface of the sphere. The spring is oriented radially and its other end is firmly anchored at a distance equal to its rest length. When P moves outward a distance u, it is subject to a force, directed radially inward, of magnitude ku. The boundary conditions for elastic motions of this body can be expressed as

$$\widehat{\mathbf{r}} \cdot \mathbb{T} = -\widehat{\mathbf{r}} k \left(\mathbf{u} \cdot \widehat{\mathbf{r}}\right) \delta \left(\widehat{\mathbf{r}} - \widehat{\mathbf{r}}_p\right) \quad \text{on } r = r_N . \tag{D1}$$

$\mathbb{T}$ is the elastic stress tensor, $\mathbf{u}$ is displacement, $\widehat{\mathbf{r}}_p$ is the location of P, δ is the surface Dirac delta function, and r_N is the sphere's outer surface. Thus, for all points on $r = r_N$ other than P, as before, $\widehat{\mathbf{r}} \cdot \mathbb{T}$ must vanish.

We now utilize Rayleigh's principle to compute, correct to first order, the perturbation $\delta\omega^2$ in an eigenvalue ω^2 caused by the perturbed boundary condition. The Fourier transformed equation of motion is

$$-\rho\omega^2 \mathbf{u} = \boldsymbol{\nabla} \cdot \mathbb{T} \tag{D2}$$

(We have dropped sub- and superscripts.) Forming the dot (scalar) product of D2 with $\mathbf{u}$ gives

$$-\rho\omega^2 \mathbf{u} \cdot \mathbf{u}^\dagger = (\boldsymbol{\nabla} \cdot \mathbb{T}) \cdot \mathbf{u}^\dagger. \tag{D3}$$

Equation D3 is true everywhere and we may integrate both sides of it over the volume $0 \leq r \leq r_{_N}$. If while doing so we rearrange the right-hand side somewhat and appeal to Gauss' theorem, we may easily arrive at

$$\omega^2 \int_V \rho \mathbf{u} \cdot \mathbf{u}^\dagger \, dv = \int_V \mathbb{T} : \boldsymbol{\nabla} \mathbf{u} \, dv - \int_S \widehat{\mathbf{r}} \cdot \mathbb{T} \cdot \mathbf{u}^\dagger \, du. \tag{D4}$$

V denotes the volume of integration and S is its surface. The colon denotes a scalar tensor product.

In the absence of a boundary perturbation the surface integral vanishes since $\widehat{\mathbf{r}} \cdot \mathbb{T}$ vanishes on S. What remains, in this case, is exactly equation 61 describing the equality of kinetic and potential energies in free vibration. To determine the effect (to first order) of the new boundary condition D1, we (following (Rayleigh, 1945)) replace ω^2 by $\omega^2 + \delta\omega^2$ and evaluate the contribution of the surface integral. We then subtract the unperturbed energy terms (which are equal) leaving

$$\delta\omega^2 \int_V \rho \mathbf{u} \cdot \mathbf{u} \, dv = k \left(\mathbf{u} \cdot \widehat{\mathbf{r}}\right)^2 \tag{D5}$$

where $\mathbf{u} \cdot \widehat{\mathbf{r}}$ is evaluated at $\widehat{\mathbf{r}}_p$.

If we adopt the normalization 78, the volume integral becomes equal to unity. If $\widehat{\mathbf{r}}_p$ is at either $\theta = 0$ or $\theta = \pi$, and if we replace $\delta\omega^2$ by $2\omega\delta\omega$, we may massage D5 into the form

$${}_n\left(\frac{\delta\omega}{\omega}\right)_l = \frac{1}{2} k \, {}_nA_l \tag{D6}$$

where ${}_nA_l$ is the appropriate source factor, and we consider only axisymmetric ($m = 0$) vibrations.

A sphere against a half-space

In order to estimate an appropriate value for the spring constant k, we consider the contact problem of a sphere against a half-space. Let E_s and V_s be the Young's modulus and Poisson's ratio of the sphere, E_n and V_n the corresponding properties of the half-space, and R the radius of the sphere. Timoshenko and Goodier (Timoshenko & Goodier, 1951) present approximate results, useful when the contact area is small, which we quote here. The normal force F, not stress, acting on the sphere causes it to move a distance d toward the half-space given by

$$d = \left(\frac{9\pi^2}{16}\right)^{\frac{1}{3}} \left[\frac{F^2}{R}\left(k_s + k_n\right)^2\right]^{\frac{1}{3}} \tag{D7}$$

where

$$k_s = \frac{1 - V_s^2}{\pi E_s}$$

and

$$k_n = \frac{1 - V_n^2}{\pi E_n}.$$

We suppose that the sphere is pressed against the support, or transducer, with a force F and that motion results in small variations about an equilibrium position given by D7. Then the appropriate value for the spring constant is given by

$$k = \left(\partial_F d\right)^{-1} \tag{D8}$$

where the derivative is evaluated at F, the confining force. We cannot expect this model to be useful if any dimensions involved become significant compared to a wavelength of motion (about $2\pi R/(l + \frac{1}{2})$). All we really ask of it, in any case, is an order of magnitude for potential errors. Equations D7 and D8 give

$$k = \frac{3}{2}\left[\frac{16RF}{9\pi^2(k_s+k_n)^2}\right]^{\frac{1}{3}} \tag{D9}$$

Another quantity of some interest is the radius a of the contact area, given by

$$a = \left[\frac{3\pi}{4}FR(k_s+k_n)\right]^{\frac{1}{3}}$$

Table DI presents numerical results from these expressions for a Lucite and a fused silica sphere, 4 in. in diameter, held by its own weight on a steel support and a polyethylene support. The elastic constants were taken from Mason (Mason, 1958). The lower portion of the table gives the effective spring constants, contact dimension, and fractional perturbations for several modes.

These results suggest that soft materials, such as polyethylene, induce a smaller shift in measured eigenfrequencies than do hard ones. We may interpret this as being due to the low acoustic impedance of polyethylene which more nearly matches the free boundary condition. As impedance increases, the effective boundary condition in the contact area approaches a rigid boundary state, and the influence on eigenfrequency grows accordingly. Equation D6 requires $\delta\omega/\omega$ to grow without bound as k goes to infinity. We must recall that D6 applies *only* to modes with $M = 0$ when the spring is affixed at one of the poles. A spring affixed to a mode's node has no disturbing influence.

We also note that, not surprisingly, modes with small source factors (such as ${}_1S_2$) are less perturbed than modes with large source factors (such as ${}_0S_2$). Since the source factor is directly related to the amplitude of surface radial displacement, such a result is to be expected. This result is not particularly helpful in choosing data since low-source-factor modes are more difficult to observe and locate accurately.

Table DI:

Material	Young's modulus	Poisson's ratio	k_s or k_n	$\frac{4\pi g}{3}\rho R^3$ for 4 in. sphere
Lucite	0.4×10^{10}	0.4	6.68×10^{-11}	8×10^5
Fused silica	7.3×10^{10}	0.17	4.24×10^{-12}	1.38×10^6
#347 Stainless	19.6×10^{10}	0.30	1.48×10^{-12}	
Polyethylene	0.076×10^{10}	0.458	3.31×10^{-10}	

Material pair	k	a	$\frac{\delta f}{f}$ ${}_0S_2$	${}_0S_0$	${}_0S_4$	${}_1S_2$
Lucite Stainless	8.1×10^8	8.7×10^{-2}	3.7×10^{-4}	2.5×10^{-5}	2.9×10^{-4}	9.0×10^{-8}
Lucite Polyethylene	2.5×10^8	0.16	1.1×10^{-4}	7.7×10^{-6}	8.9×10^{-5}	2.7×10^{-8}
Fused silica Stainless	5.1×10^9	4.5×10^{-2}	2.0×10^{-4}	2.9×10^{-5}	1.7×10^{-4}	6.0×10^{-6}
Fused silica Polyethylene	3.3×10^8	0.18	1.3×10^{-5}	1.9×10^{-6}	1.1×10^{-5}	3.9×10^{-7}

E Graphical Inversion Aids

[1996 Note: In the original, these figures were printed on large, separate sheets.]

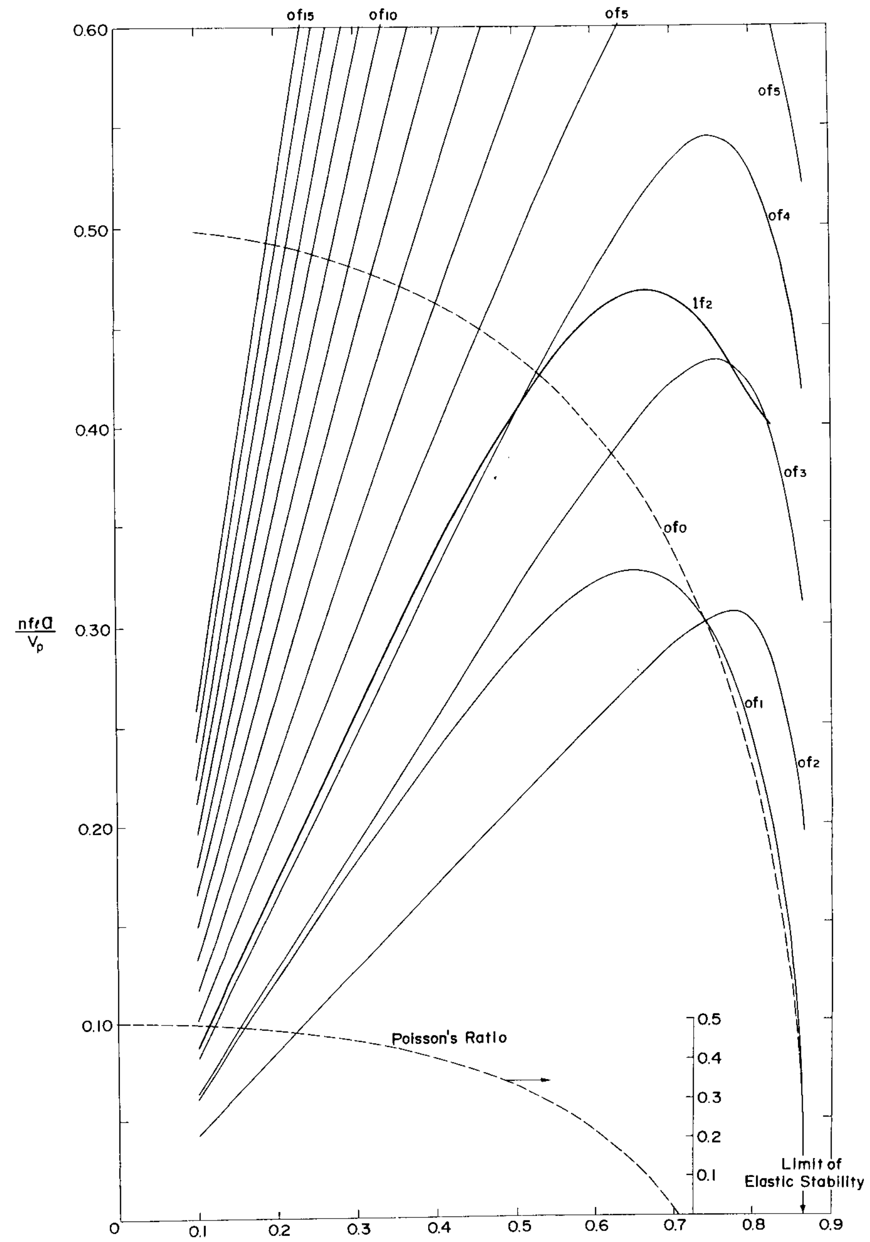

of15
of10
of5
of5
of4
1f2
of3
of0
of1
of2
0.60
0.50
0.40
0.30
0.20
0.10
0
0.1
0.2
0.3
0.4
0.5
0.6
0.7
0.8
0.9
$\frac{nfa}{V_p}$
V_s/V_p
Poisson's Ratio
0.5
0.4
0.3
0.2
0.1
Limit of
Elastic Stability

Figure E1:

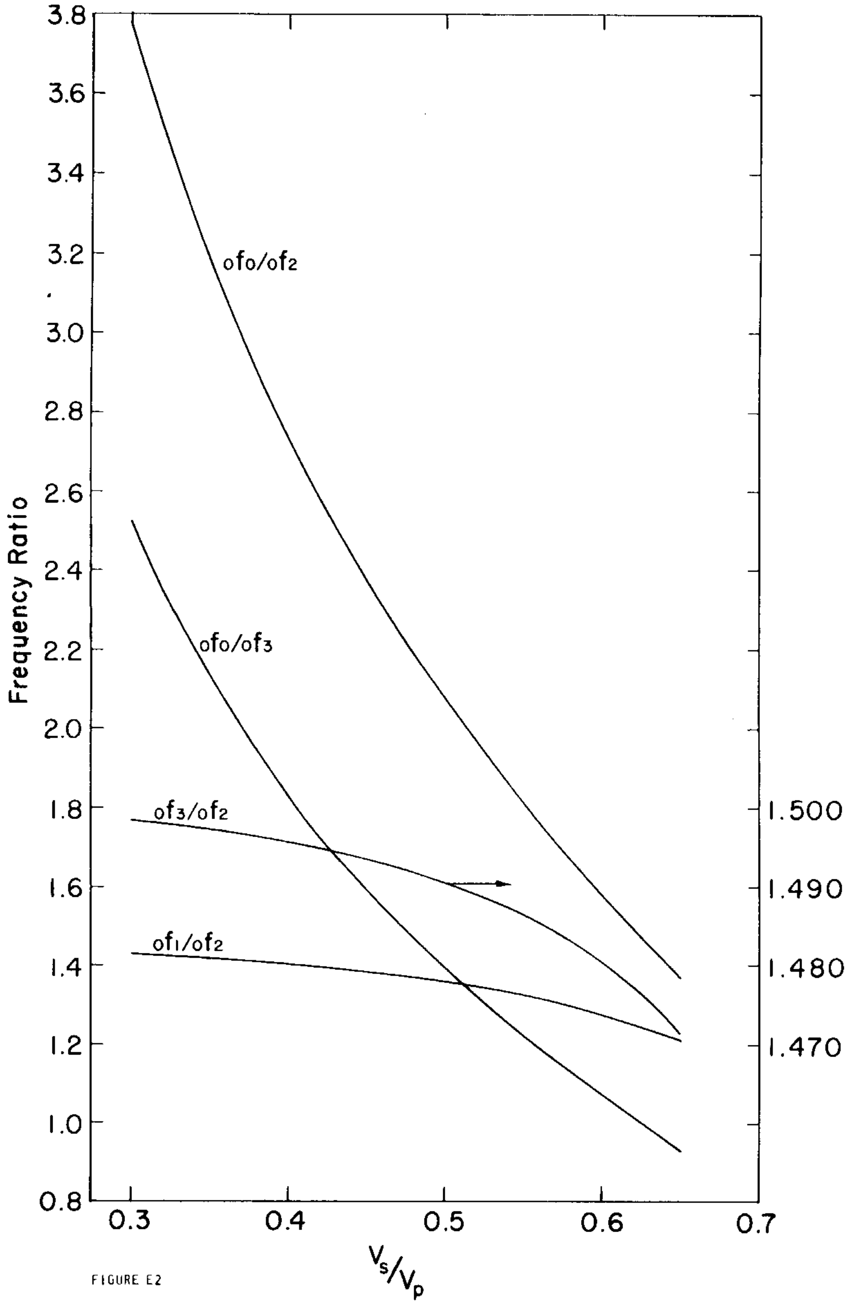
3.8
3.6
3.4
3.2
3.0
2.8
2.6
2.4
2.2
2.0
1.8
1.6
1.4
1.2
1.0
0.8
Frequency Ratio
ofo/of2
ofo/of3
of3/of2
of1/of2
1.500
1.490
1.480
1.470
0.3
0.4
0.5
0.6
0.7
Vs/Vp
FIGURE E2

Figure E2: